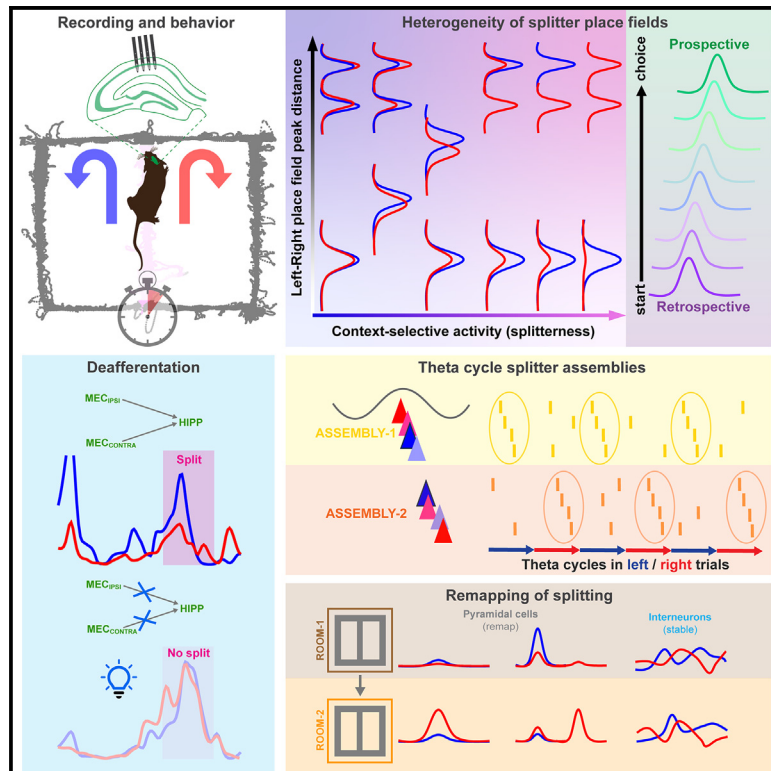# Working memory features are embedded in hippocampal place fields

Graphical abstract

Authors

Viktor Varga, Peter Petersen,
Ipshita Zutshi, Roman Huszar,
Yiyao Zhang, György Buzsáki

Correspondence

gyorgy.buzsaki@nyulangone.org

In brief

Varga et al. show that memory and place field features of both pyramidal cells and interneurons in the hippocampus are interchangeable. Optogenetic suppression of the medial entorhinal input decreases the fraction of choice-predicting neurons.

Highlights

- Memory and place field features of hippocampal neurons are a continuum

- Retrospective and prospective firing can vary even within a single field

- Interneurons also exhibit splitter activity preserved in a novel environment

- Bilateral medial entorhinal inactivation decreases the fraction of splitter cells

Article

Working memory features are embedded in hippocampal place fields

Viktor Varga,[1,2] Peter Petersen,[1,3] Ipshita Zutshi,[1] Roman Huszar,[1] Yiyao Zhang,[1] and György Buzsáki[1,4,5,6,*]

[1]Neuroscience Institute, Langone Health, New York University, New York, NY, USA
[2]Subcortical Modulation Research Group, Institute of Experimental Medicine – Hungarian Research Network, Budapest, Hungary
[3]Department of Neuroscience, University of Copenhagen, Copenhagen, Denmark
[4]Department of Neuroscience and Physiology, Langone Health, New York University, New York, NY, USA
[5]Department of Neurology, Langone Health, New York University, New York, NY, USA
[6]Lead contact
*Correspondence: gyorgy.buzsaki@nyulangone.org
https://doi.org/10.1016/j.celrep.2024.113807

SUMMARY

Hippocampal principal neurons display both spatial tuning properties and memory features. Whether this distinction corresponds to separate neuron types or a context-dependent continuum has been debated. We report here that the task-context ("splitter") feature is highly variable along both trial and spatial position axes. Neurons acquire or lose splitter features across trials even when place field features remain unaltered. Multiple place fields of the same neuron can individually encode both past or future run trajectories, implying that splitter fields are under the control of assembly activity. Place fields can be differentiated into subfields by the behavioral choice of the animal, and splitting within subfields evolves across trials. Interneurons also differentiate choices by integrating inputs from pyramidal cells. Finally, bilateral optogenetic inactivation of the medial entorhinal cortex reversibly decreases the fraction of splitter fields. Our findings suggest that place or splitter features are different manifestations of the same hippocampal computation.

INTRODUCTION

In addition to their well-studied spatial tuning properties,[1,2] hippocampal neurons also possess memory features (for reviews, see Duvelle et al.[3] and Hasselmo and Eichenbaum[4]). A particular form of activity occurs when a rat runs repeatedly through the same location but neurons fire at different firing rates biased by working memory demands.[5] Such differential spiking patterns, colloquially referred to as "splitter" fields,[6–8] are typically quantified in the central arm of a maze, and the differential firing patterns of neurons on correct and error trials can distinguish either the past or future run paths of the animal (referred to as "retrospective" or "prospective" splitter fields[7,9]).

The discovery of splitter cells signaled a conceptual departure from the spatial navigation view of the hippocampus, and splitter fields appeared to provide an entry point for the physiological examination of the memory function of the hippocampus.[3,10,11] Splitter neurons[4,7,12–16] have been used to study context- and schema-dependent activity,[5,17,18] journey dependence,[9,19–21] "policy-" or goal-related activity,[22] and trajectory coding,[23–25] but they refer to the same internally organized process, as opposed to place cells, whose firing fields are traditionally believed to "represent" particular constellations of the currently perceived environment.[1] This departure from the spatial mapping view of the hippocampus led to the tacit assumption that there are (at least) two functional types of neurons in the hippocampus, place cells and splitter (memory) cells, although such division did not lead to the identification of special and distinct features of the alleged different types. In fact, the fraction of splitter cells varies extensively across studies (for review, see Duvelle et al.[3]), and the questions remained whether all hippocampal neurons can show both place fields and memory fields and whether it is only the experimental conditions that bias the expression of place or memory features. A recent challenge to the memory function of hippocampal neuronal firing comes from a report that suggests that splitter features of hippocampal pyramidal neurons are inherited from the prefrontal cortex and conveyed directly to the hippocampus via the nucleus reuniens of the thalamus.[25] In addition, an influential recent review concluded that non-spatial firing features are, in fact, secondary manifestations of the spatial map.[26]

Given the conceptual importance of the splitter (memory) feature of neuronal spiking, we reexamined the relationship between place fields and splitter fields. Because previous studies already suggested that the fraction of splitter fields is affected by the delay between responses in a spatial alternation task,[5] we trained two groups of mice with and without delays in one or two environments and examined firing characteristics of both pyramidal cells and interneurons. We demonstrate a continuum of place fields and splitter fields. To address the inheritance issue, we reversibly disconnected the hippocampus from its upstream medial entorhinal input and found that bilateral inactivation of upstream inputs decreased the fraction of splitter neurons in the hippocampus.
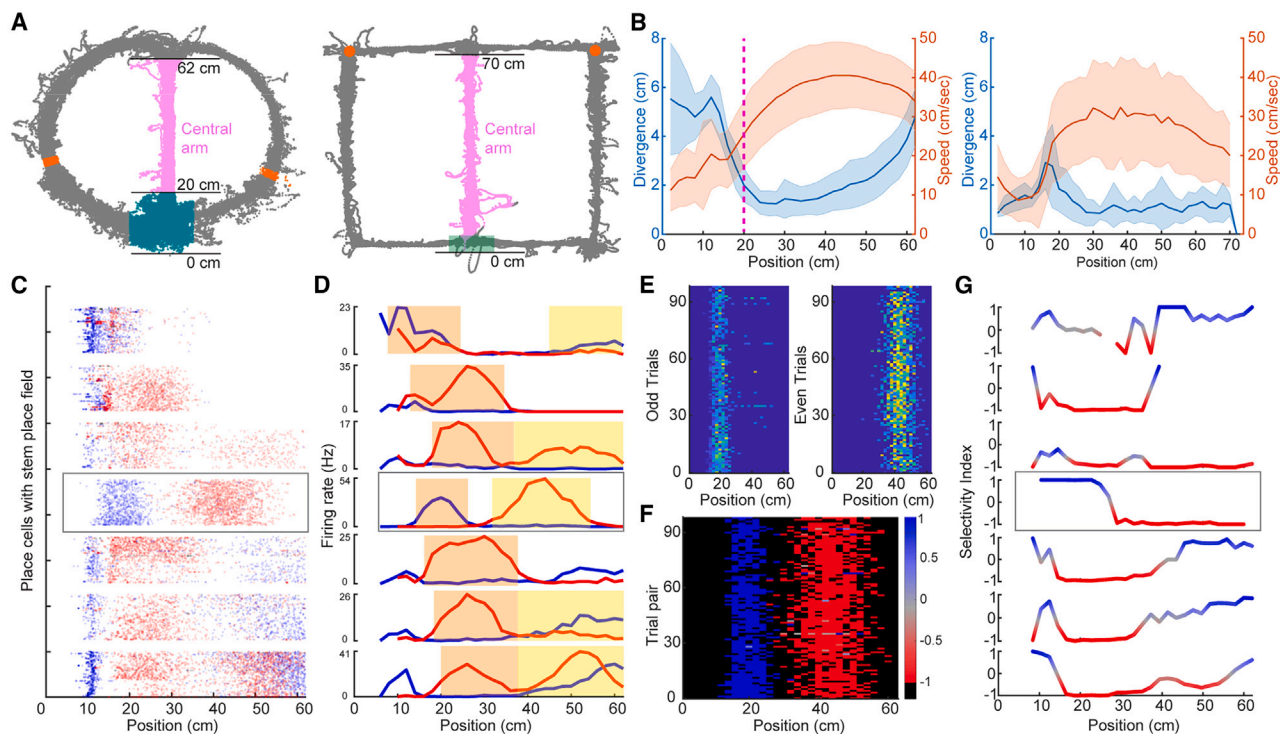
Figure 1. Context-selective spiking activity in spatial alternation tasks

(A) Superimposed travel trajectories of two example mice in a continuous alternation task session and a delayed alternation task session, respectively. Central arm (pink), transition zone (green), reward areas (red), and delay zone (light, semi-transparent green) are indicated.

(B) Divergence of travel trajectories in left versus right trials (blue) and speed (red) in the central arm calculated in 2-cm spatial bins. The vertical line at 20 cm (left plot) marks the start of the central arm in calculations of continuous sessions (0–20 cm was designated as a transition zone).

(C) Place/splitter fields in the central arm in an example session of the continuous alternation task. Spikes during left and right trials are marked by blue and red dots, respectively.

(D) Tuning curves (TCs) of place cells (PCs) shown in (C). Orange and yellow boxes mark place fields. The neuron marked by the gray rectangles in (C) and (D) are further analyzed in (E) and (F).

(E) Left and right spiking activity per trial of the neuron. Color-coded FR: firing rate.

(F) Selectivity index (SI) per trial, calculated from spike rate difference in non-overlapping left/right trial pairs for each spatial bin (see Figure S1 for details). Blue and red represent left and right turn predictions, respectively.

(G) Color-coded SI as a function of the animal's position on the maze. Note the flip of the SI at different positions in the central arm.

RESULTS

Neurons from the hippocampal CA1 region were recorded with multiple-shank silicon probes in mice (n = 9) while they performed in a rewarded spatial alternation task in a modified figure-8 maze (Figure 1A).[27] One group was trained to complete at least 40 alternations (n = 5 mice, 128 ± 34 trials) without delay (continuous task), whereas a 5-s delay was introduced for the other group (delayed task: n = 4 mice, 30 ± 8 trials). Well-isolated neurons were separated into putative pyramidal cells and interneurons based on their spike count and autocorrelation[28] (STAR Methods). The x-y-z position of the animal's head was monitored with a 6-camera motion capture system (continuous task)[29] or by an overhead camera (delayed task), which showed that the animal's head position during left and right trials varied less than 2 cm in the central arm (Figure 1B; median, interquartile range [IQR]: 1.7, 2.2 cm).

Based on a double-threshold place field detection (see STAR Methods), 2,412 of 2,912 putative pyramidal cells had a place field on the maze, of which 1,225 possessed a place field in the central arm (see Figure S3 for the distribution of place fields; Table S1). Our analyses were confined to neurons that had place field peaks in the central arm. Figures 1C, 1D, and 1G illustrate seven central arm place cells recorded in a single continuous alternation session, with spikes during left and right trials shown in blue and red, respectively. The firing rates and spatial occupancy of the spikes were distinct on left and right trials (referred to as "context" in this paper),[25,30] identifying them as splitter cells.[6,7] To quantify this left/right asymmetry, we utilized different measures for single-neuron analyses (see Figure S1 for details). First, we introduced a "selectivity index" (SI) with values 1 and –1 corresponding to maximum arm-choice selectivity by calculating a "change ratio" [(a + b)/(a − b)] based on non-overlapping, consecutive trial pairs (i.e., 1–2, 3–4, 5–6, 7–8, …; −1 or 1 can be either left or right, depending on whether the 1st trial was right or left, respectively; see STAR Methods for further details). SIs were used to create an "SI map," enabling the analysis of context-correlated activity along both the spatial (bin) and trial
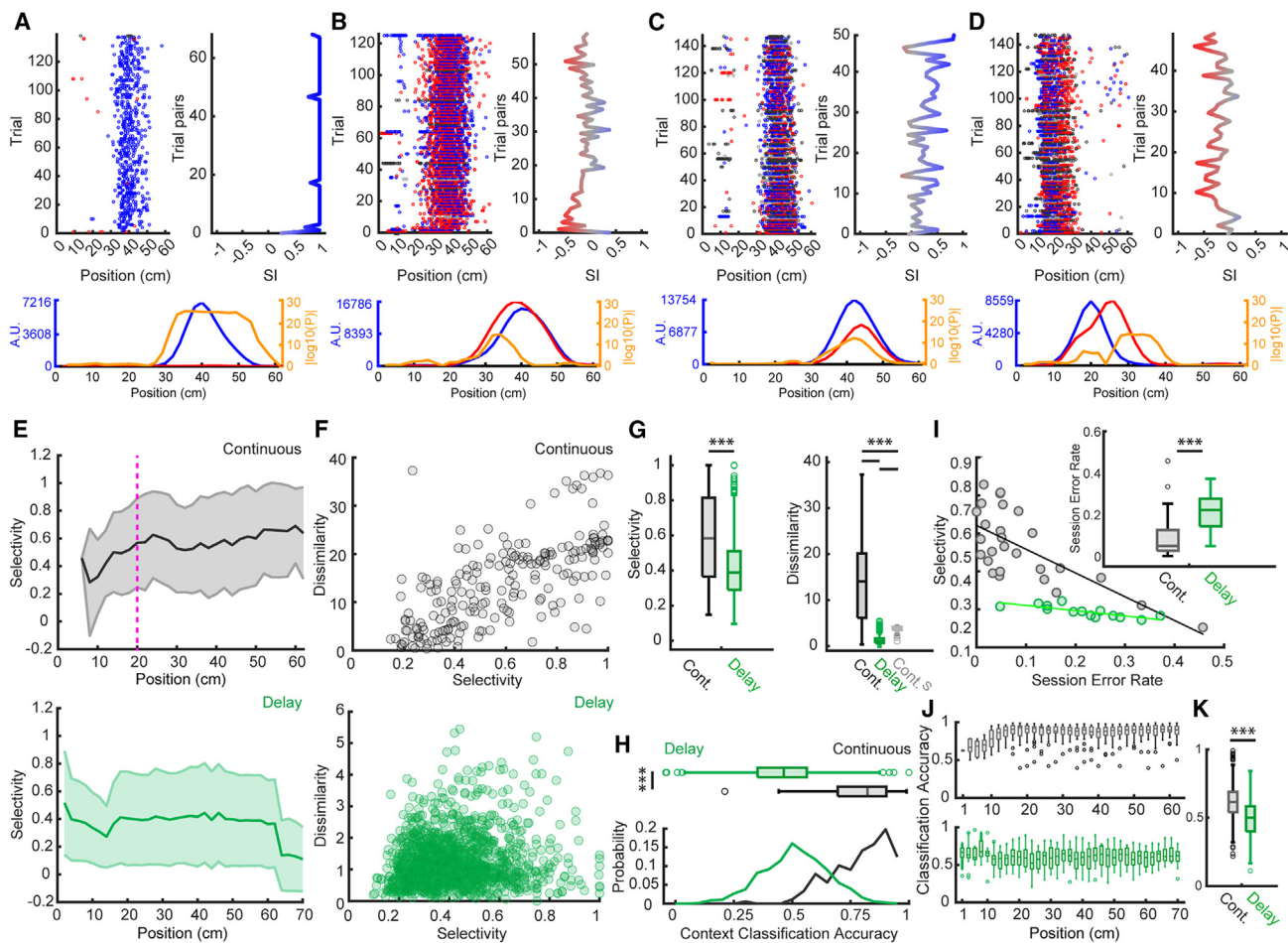
Figure 2. Context selectivity is a continuum

(A–D) Example neurons with varying degrees of context selectivity: highly selective (splitter, A) and moderately selective (B–D) pyramidal cells. Top plots: position – trial rasters (blue dots: left trial spikes, red dots: right trial spikes) and trial-by-trial selectivity (right); bottom plots: separate left and right trial TCs and their bin-by-bin difference by Wilcoxon rank-sum test, termed dissimilarity (blue, red, and orange lines, respectively).

(E) Position-dependent average selectivity of place fields in the continuous (top) and delayed (bottom) tasks (mean ± SD is shown). The vertical dashed line marks the beginning of the central arm in the continuous task.

(F) Selectivity plotted against within-place field left-right firing rate difference of TCs (absolute value of log p values as the orange lines in A–D; dissimilarity).

(G) Both selectivity and dissimilarity are significantly higher in the continuous alternation versus delayed task, even if only a matching number of randomly selected continuous trials (C^S) was used for the comparison (n = 206 place fields in continuous versus n = 1,342 place fields in delayed; Wilcoxon rank-sum test, ***p < 0.001).

(H) Distribution of context classification accuracy (1 – false classification rate) based on both infield and outfield activity (see Figure S1). The goodness of predicting correct trials is based on classification of TCs by an ensemble-bagged tree classifier, which was higher in the continuous alternation task (n = 177 and 1,048 neurons in continuous and delayed alternation tasks, respectively; Wilcoxon rank-sum test, ***p < 0.001).

(I) Error rate (proportion of error trials) was lower in continuous compared to delayed alternation task (inset: n = 27 continuous versus n = 14 delayed alternation sessions; Wilcoxon rank-sum test, ***p < 0.001), and the session error rate was inversely correlated with selectivity (continuous: R = −0.7, p < 0.0001; delay: R = −0.79, p < 0.0001).

(J) Position-resolved context selectivity quantified by population vector analysis using population vectors as inputs of the context classifier.

(K) Mean population-vector-based context selectivity in every session. Median, interquartile, and 10–90 ranges and outliers are shown (n = 27 continuous sessions by 31 spatial bins and n = 14 delayed sessions by 35 spatial bins; Wilcoxon rank-sum test, ***p < 0.001).

number dimensions (Figures 1F and 1G). Additionally, selectivity without side direction information, defined as the absolute value of SI (range: 0–1), was used as a global measure of context-correlated activity independent of the trial-by-trial or in-field fluctuations. Second, we calculated the bin-by-bin difference of firing rate in left versus right trials by a non-parametric unpaired test (Wilcoxon's rank-sum test) and used the negative logarithm

of the p value as a "dissimilarity index" (Figures 2A–2D and 3A–3F, bottom plots), which quantified the significance of side preference along the spatial axis. Third, we also determined how accurately the left or right choice (context) of the mouse could be predicted by an "ensemble-bagged tree classifier" using single-trial tuning curves as predictors, a measure that served to quantify how well contextual information (i.e., side

choice) is reflected by the trial-by-trial fluctuation of activity (Figure S1).

Conjunctive place and predictive properties of splitter cells

The classical definition of splitter cells is based on firing rate differences between left and right trials, emphasizing their distinct memory features separate from place cells.[6,7] In contrast to this distinction, we observed a continuum between classical place and splitter cells in both tasks, indicating that the term splitter field depends on an arbitrary threshold. The magnitude of the SI varied as a function of both firing rate difference and the spatial separation of left and right trial fields along the direction of run (see Figure 1G). Within the same field, rate could vary from maximum firing in one direction to virtually no firing when the mouse turned in the opposite direction (Figure 2A; classical splitter neuron). Yet, left and right firing fields of the same neuron, even with similar peak rates but with some spatial offset, yielded significant selectivity and dissimilarity (Figures 2B–2D). Both measures were higher and correlated with each other in the continuous, but not in the delayed, task (Figures 2E, 2F, S3E, and S3G). The magnitudes of selectivity were similar along the central arm in both versions of the task. The behavioral choice could be better predicted in the continuous than the delayed task on the basis of trial-by-trial tuning curves (Figure 2H). As expected, selectivity inversely correlated with error rate in both tasks but more so in the continuous version (Figure 2I). Population vector analysis (see STAR Methods) could also accurately predict behavioral choice, especially in the continuous task (Figures 2J and 2K; see further analyses in Figure S1). Importantly, selectivity did not depend on the lateral (left-right) position of the mouse in the central arm (Figures 1B and S3B).[6]

The SI varied not only as a function of position in the central arm but as a function of trial number as well (Figure S4). Similar to true place fields, many splitter fields were present on the first trial and remained stable throughout the entire session (Figures 2A and S4A). However, a minority of splitter cells developed or changed their context selectivity gradually or abruptly (Figure S4C). Another minority expressed both their place fields and SIs during early trials but switched side preference in later parts of the session (Figure S4B). Fluctuations of SI and firing rate were often decoupled within place fields (Figures S4D–S4F). The context selectivity of spikes could not be explained by unit classification error (Figure S2).

Properties of splitter cells with multiple place fields

A number of place cells possessed two or more place fields (28% in the continuous alternation task; 37% in the delayed task). We tested how splitter features are distributed across two or more place fields of the same neuron. Most dual-field neurons possessed splitter fields, and, unexpectedly, the two place fields often exhibited opposite context preference (Figure 3A). Thus, the SIs of the two fields could vary even within the same trial (Figure 3K). Uncorrelated context selectivity of dual-field neurons was also observed, i.e., when one place field of a place cell was judged as non-splitter, the second place field of the same neuron could display splitter feature (Figure 3B). In rare cases, both fields were biased to the same side (Figure 3C).

The firing rates of the two place fields could differ or be nearly identical (Figures 3A–3E), illustrating that simple spike count differences cannot reliably identify splitter cells. Dual place field neurons had similar level of selectivity as neurons with single place fields (Figure 3G; median, IQR: 0.76, 0.51 versus 0.47, 0.6; p = 0.85, Wilcoxon's rank-sum test). Thus, each place field can have its distinct splitter characteristics.

While the distinction of single versus dual place fields is simple when place fields are far apart, it becomes problematic when place fields "fuse" together.[31] Separation of left and right trials could address this issue, and, as a result, seemingly single place fields revealed their dual nature when characterized by SI and dissimilarity index. For example, plotting tuning curves of left and right trials separately of the large place field of the neuron shown in Figure 3E revealed fused double fields or subfields. Another example neuron (Figure 3F) had a higher firing rate in the first few bins of right trials, whereas in the remaining bins of the field, it was non-selective. The distribution of distances between the peaks of left and right subfields was skewed, with significantly larger distances between subfields in the continuous than in the delayed task (Figures 3H and 3I). To characterize within-field context switching further, we calculated the difference between the maximum and minimum SIs within place fields. If the entire field is biased only to one side (i.e., a simple splitter field), then min(SI) and max(SI) will have the same sign. If min and max have opposite signs, it is an indication of switching selectivity. This quantification revealed that a considerable fraction of place fields exhibited dual-context selectivity (transiently predicting one and then the other arm; dots concentrated in the top left corners of Figure 3J), although, as expected, the average of SIs of the switching fields was lower (blueish color) than that of the side preference of consistent splitter cells. The majority of double place field neurons in the continuous, but not delayed, task predicted opposite choice directions (Figure 3K). In summary, side prediction is not a consistent feature of neurons because splitter fields can differ across multiple fields and even within the same field across different trials.

Error trials reveal dynamically changing splitter features

Spiking activity during error trials helped us disambiguate whether the splitter fields matched future (prospective) or past choices (retrospective[7]; reviewed in Dudchenko and Wood[12]). Four template firing fields were constructed from correct and erroneous left and right trials. In the example shown in Figures 4A–4F, templates of correct right and left trials matched erroneous left and right trials, respectively, implying that splitter fields in this case reflected past behavioral choices (retrospective[7]). However, the retrospective or prospective signature of a given neuron was not fixed. Spatial bin-by-bin comparison of the tuning curves revealed that the prospective and retrospective nature of place fields could change ("flip") even within the same place field of the neuron (Figures 4F and 4G). Firing fields of dual place field neurons often had opposite (prospective versus retrospective) correlations (Figures 4H and 4I). In the continuous task, retrospective fields were, overall, more frequent than prospective fields (Figure 4J). However, while retrospective fields dominated the initial part of the central
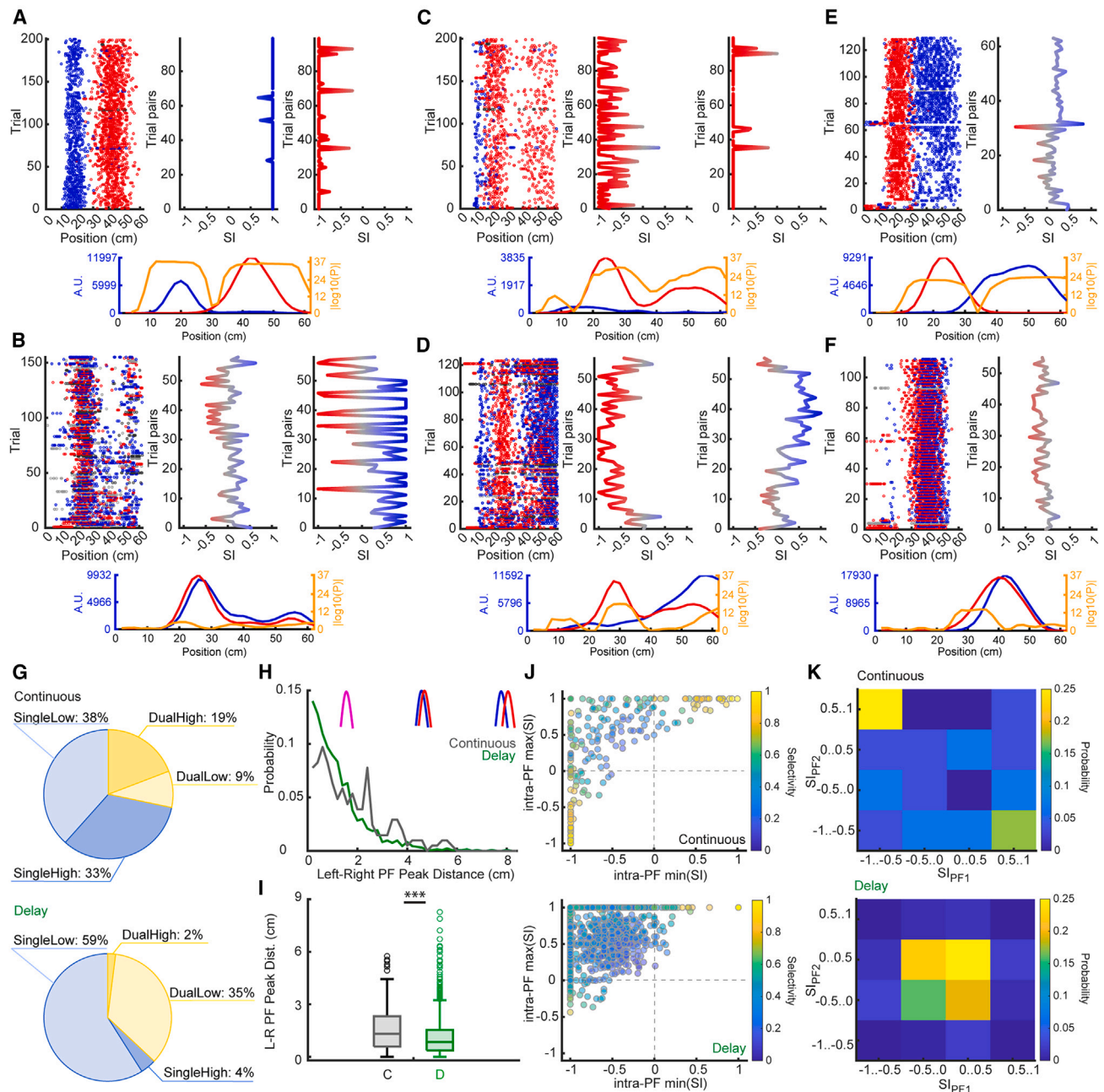
Figure 3. Neurons with multiple splitter fields

(A–F) Spike raster plots (left) and trial-by-trial selectivity plots (right) of dual and "complex" field PCs. Example neurons with opposite-side-selective (A), non-selective (B), same-side-selective (C), and variably selective (D) fields.

(E and F) Single place field cells with largely separate (E) and highly overlapping (F) left and right firing fields. Bottom: left (blue) and right (red) smoothed TCs and their position-dependent difference by Wilcoxon rank-sum test (orange, dissimilarity).

(G) Proportion of context-independent (low; $|SI| \leq 0.5$) and context-selective (high; $|SI| > 0.5$) place fields of dual and single field neurons (continuous task, n = 206 fields; delayed task, n = 1,342 fields).

(H) Distribution of distances between left and right subfield peaks in continuous and delayed alternation tasks.

(I) Median and interquartile range plus outliers of subfield peak distances (Wilcoxon rank-sum test: ***p < 0.001).

(J) Context-changing fields, quantified by the maximum-minimum SI values within place fields. If min and max have opposite signs (top left quadrant), then the SIs switched within field (see Figure S1).

(K) Joint distribution of SI in place field 1 (PF1) versus PF2 for dual field neurons. In the continuous alternation task, the two fields mainly predicted opposite choices (as in the example neuron in A). In the delayed task, the two fields were more similar. PF1 and PF2 are anti-correlated in the continuous but uncorrelated in the delayed task (continuous: R = − 0.58, p = 0.0011; delayed: R = 0.07, p = 0.27).
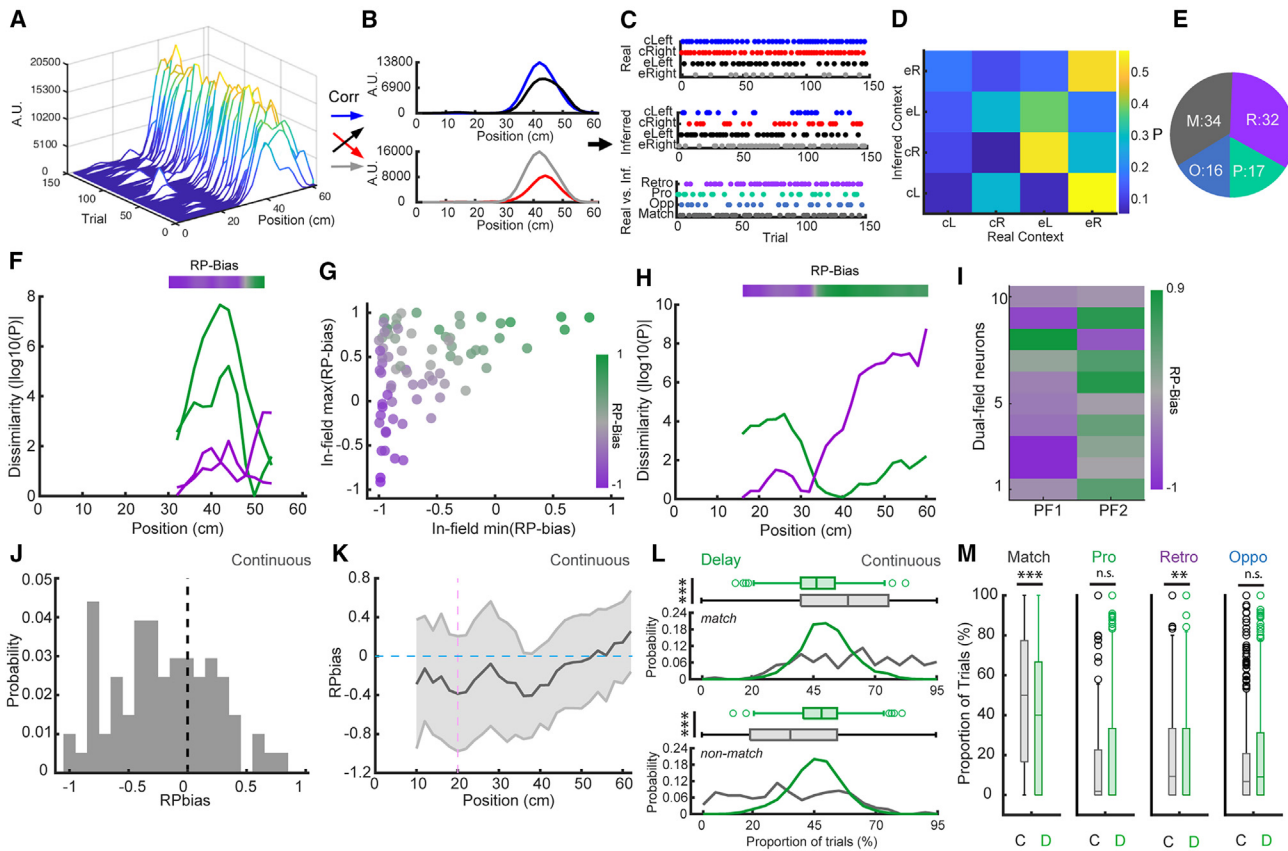
Figure 4. Relationship between neuronal activity and behavioral choice

(A–E) Calculation of neural and behavioral state correlations based on correct and error TC templates.

(A) TCs of a neuron for 150 trials.

(B) Average TCs were constructed separately for each trial type (correct left, correct right, error left, and error right trials), yielding 4 trial-type templates. Next, every single trial TC was correlated with these templates, resulting in 4 correlation values for each trial. The highest correlation was selected ("trial type"), and the trial type it corresponded to was assigned to the given trial as inferred trial type/context.

(C) Trial-type classification. Top: trials are marked by the animal's choices (real context). Middle: trials are marked based on the best-matching TCs. Bottom: marking trials based on neuronal template when behavioral choice matches its template (match), trials when behavioral and spiking-inferred choices are opposite (opp), trials when behavioral choices are best predicted from the template of upcoming choice-correlated activity (prospective, pro [P]) or past choice (retrospective, retro [R]).

(D) Correlations between behavioral and neuronal template prediction. Values of the matrix correspond to probability that the animal was in Trial$_i$ while the neuron's activity best resembled Trial$_j$. Note that in this session, there were many mismatches between behavioral and best neuronal template-predicted choices.

(E) Distribution of trial types.

(F) Within-field dynamics of dissimilarity index (as the orange lines in Figures 3A–3F but here between trial types indicated on the plot label) for an example single field neuron. Green and purple curves correspond to correlation with future (pro) and with past (retro) choice. Minimum dissimilarity determines dominant correlation. A R-P bias ranging from −1 (R) to 1 (P) was defined based on dissimilarity (see STAR Methods).

(G) Distribution of minimum versus maximum within-field RP-bias values. Dots concentrated in the top left corner correspond to fields in which R-P bias flipped from R to P, or vice versa, within the PF. Color of dots reflects mean field R-P bias.

(H) Example dual-field neuron with different R-P biases in its two fields.

(I) Mean in-field RP-bias for all dual-field neurons from sessions with ≥5 error trials (PF1 and PF2). Neurons 1, 6, 8, and 9 have opp RP-biases in their two fields.

(J) Distribution of R-P biases for all fields (n = 206) in continuous sessions showing that the majority of fields were R.

(K) Distribution of within-field mean R-P bias in the central arm (n = 206 fields; mean ± SD). Note that the initial R correlation becomes P for the population near the end of the central arm (Kruskall-Wallis test with position bin as factor: χ^2 = 92.54, p < 0.0001).

(L) Distribution of proportion of trials with a match (top) and mismatch (bottom) between behavioral choice and predicted choice from best template.

(M) Proportions of matching, opp, P, and R trials in the continuous (gray) and delayed alternation (green) tasks.

arm, they gradually developed a prospective bias closer to the T junction (Figure 4K). The number of trials in the delayed task was generally too few to perform the above analyses. The template firing fields constructed from correct left and right and erroneous left and right trials showed that in the majority of tri-

als, the side arm choice of the mouse could be reliably predicted from the matching firing fields (Figures 4L and 4M). This finding was further corroborated by applying a classifier to all tuning curves (Figures S5A–S5C). In addition, our analysis of the population vectors of neurons added further support for
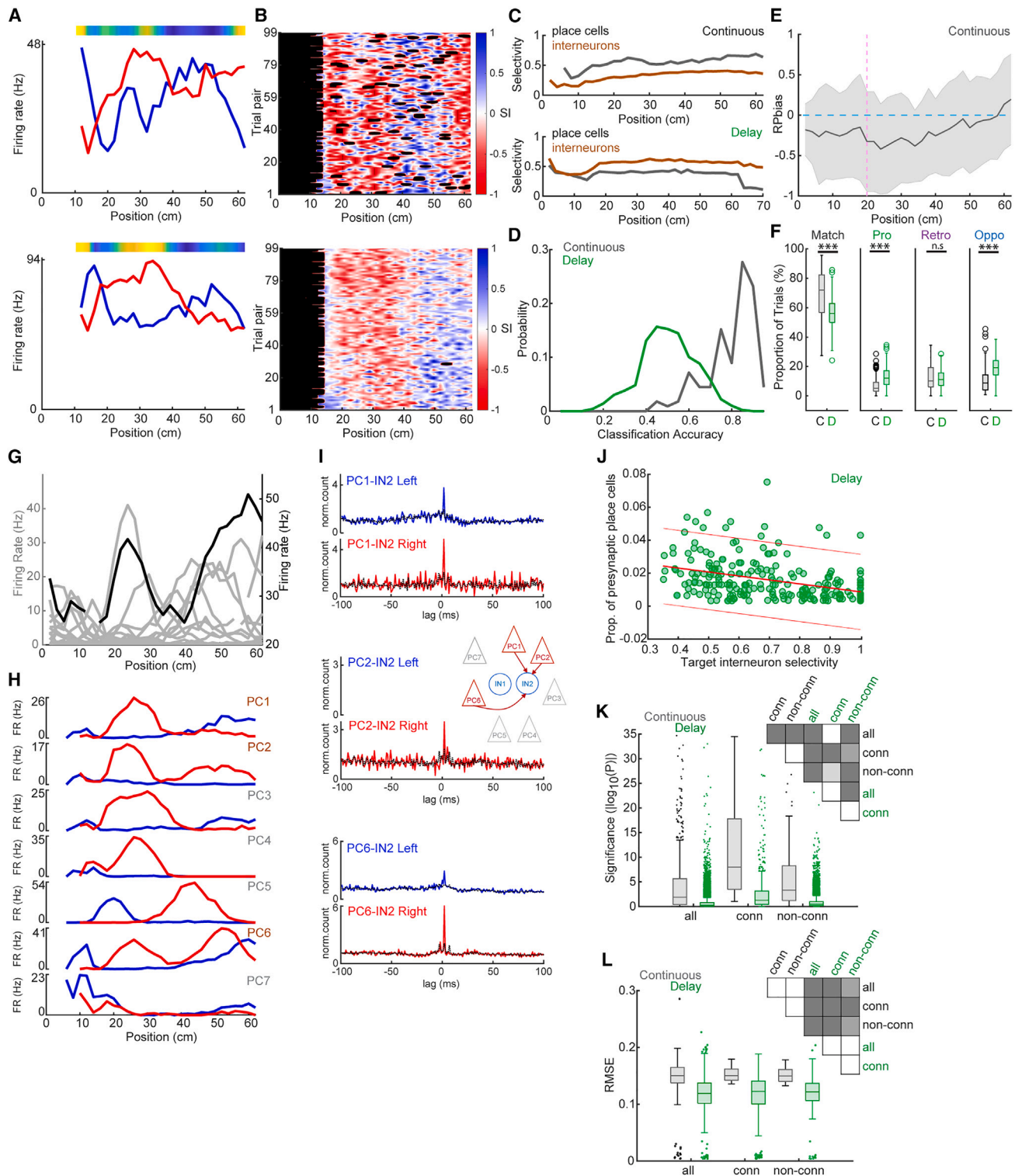
Figure 5. Context selectivity of interneurons

(A) Mean TCs in left/right trials of two example interneurons. Difference between the left versus right TCs is shown as a color-coded strip above the plots (the more yellow the color, the more dissimilar neuronal activity is in left versus right trials).

(B) SI maps of the two example interneurons.

(C) Distribution of selectivity of pyramidal (place) cells and interneurons in the central arm. Note the higher selectivity of interneurons relative to pyramidal cells in all spatial bins in the delayed task.

(legend continued on next page)

the single neuron quantifications (Figures S5G–S5K). In summary, not only could comparison of the four distinct splitter templates classify firing fields as retrospective or prospective, but we also found that the initially dominant retrospective fields gradually became prospective as the animal approached the T junction of the maze.

Choice predicting theta cycle-cell assemblies

Since the spatial position of the animal can be decoded from theta cycle population vectors,[32] we asked whether population vectors can also predict the mouse's choice. Toward that goal, we implemented a template-matching decoding algorithm. First, we confirmed that theta cycle population vectors predicted the animal's spatial position (Figure S6A; decoding error, median, IQR: 12.85, 42.83 cm and 2.45, 2.85 cm for continuous and delay sessions, respectively). Left and right choice templates as well as context-independent (non-selective) templates were constructed, and each theta cycle was classified as "unbiased" (i.e., context independent), left-biased, or right-biased based on the best template-position correlation estimate (Figures S6B and S6C; see STAR Methods). The proportion of context-biased theta cycles was uniformly distributed in the central arm in both the continuous and the delayed tasks (Figures S6G and S6H). Thus, both spatial and contextual information could be decoded from theta cycle population vectors.

We also tested whether context-correlated (i.e., choice-predicting) population vectors, composed of co-active place cells, could be detected in single theta cycles[33] and found that uniquely different assemblies were activated in left and right trials (Figures S6D and S6E). However, the assembly context selectivity, expressed as dissimilarity between average reactivation strength in left versus right trials, was not correlated with selectivity of center arm neurons (Figure S6F). Additionally, higher dissimilarity of reactivation was detected in the continuous task, whereas it was uniformly low in the delayed task (Figure S6I). Thus, while theta cycle population vectors could be used to estimate future behavioral choice, the magnitude of that estimation was poorer in the delayed task.

Choice predicting properties of inhibitory interneurons

Since several interneuron types can "inherit" some behavioral properties from their presynaptic partners, including place fields and theta phase precession,[34–36] we asked if firing patterns of interneurons can also report behavioral choice. A fraction of interneurons showed significantly different firing rate profiles in the central arm, i.e., they were splitter interneurons (Figures 5A and 5B; further examples are shown in Figures S7A–S7D). Similar to pyramidal cells, interneurons in the continuous task had higher selectivity and classification accuracy than in the delayed task (Figures 5C and 5D). The retrospective-prospective bias of interneurons in the continuous task also increased as the mouse approached the T junction of the maze (Figure 5E), and in most trials, the behavioral outcome correlated with the corresponding neuronal matching template (Figure 5F), again similar to pyramidal cells. Inspection of the spiking activity suggested that the firing patterns of interneurons in the maze largely followed the place fields of simultaneously recorded pyramidal neurons (e.g., Figure 5G). Accordingly, trial-by-trial fluctuation of interneuron activity could be predicted from the simultaneously recorded place cell firing in the central arm, especially when only the monosynaptically connected subset of pyramidal cells was used for prediction (Figures 5K and 5L and S7E–S7H). Besides firing rate fluctuation, place cell selectivity could also be used to predict the context-dependent firing of interneurons. Notably, firing-rate- and selectivity-based predictions were not correlated, indicating that different mechanisms are responsible for the dynamics of firing rate and splitter activity. To gain more insight into the place-context features of interneurons, we quantified monosynaptic connections and spike transmission probabilities between pyramidal cell-interneuron (P-I) pairs (Figures 5H–5J and S7G).[37] Spike transmission probability between P-I pairs varied between left and right trials, i.e., they were splitting P-I pairs (e.g., Figure S7I). At the

(D) Trial classification accuracy based on the presented interneurons' activity in correct left and right trials (n = 112 continuous versus 498 delayed, Wilcoxon rank-sum test: p < 0.001).

(E) In the continuous task, location-resolved distribution of R/P activity quantified as RP-bias (−1: full R, 0: unbiased, 1: P; Kruskall-Wallis test with position bin as factor: χ^2 = 167.48, p < 0.0001).

(F) Proportion of different types of neuronal-behavioral state relationships (Wilcoxon rank-sum test: ***: p < 0.001; compare with Figure 4M).

(G) TC of an interneuron and 17 simultaneously recorded pyramidal cells in an example continuous session.

(H) TC averages of seven PCs (PC1–PC7) simultaneously recorded with interneuron 1 (IN1) and IN2 of (A) in correct left and right trials in a continuous session (same PCs as in Figures 1C and 1D).

(I) Putative monosynaptic connections between three of the PCs (PC1, PC2, and PC6) and IN2. Note that PC2 did not fire enough spikes in left trials to generate the cross-correlogram. Here, the significance of putative monosynaptic connections was tested against surrogate cross-correlograms generated by randomly shifting interneuron spike times by up to 5 ms repeated 1,000 times. Black dashed line marks p = 0.01. PC3, PC4, PC5, and PC7 were not connected to IN2, and none were connected to IN1.

(J) Selectivity of all recorded interneurons plotted against the proportion of putative presynaptic pyramidal cells relative to all pyramidal cells in delay sessions (R = −0.51, p < 0.001, top and bottom lines correspond to 95% prediction interval).

(K) Contribution of PCs to the activity of simultaneously recorded interneurons was calculated for all sessions by a linear regression model (P = probability that the model was significantly different from a model with constant regressors). Plots show median, quartile range, non-outlier range, and outliers as dots. all, all PCs were used in the model; conn, only PCs with putative monosynaptic connections were used; non-conn, PCs with no detectable connections were fed into the regression. Differences among the 6 groups (3 models * 2 types of task) were significant by Kruskal-Wallis ANOVA, X^2 = 863.82, p < 0.001; significant differences by Tukey's honestly significant difference procedure are shown in the checkerboard: shades of gray (dark to light) = p < 0.001, 0.001 < p < 0.01, and 0.01 < p < 0.05.

(L) Root-mean-square error (RMSE) of all models (all, connected, and non-connected PCs). Difference among the 6 groups (3 models * 2 types of task) by Kruskall-Wallis ANOVA, X^2 = 118.6, p < 0.001, significance of pairwise differences is shown on the checkerboard.
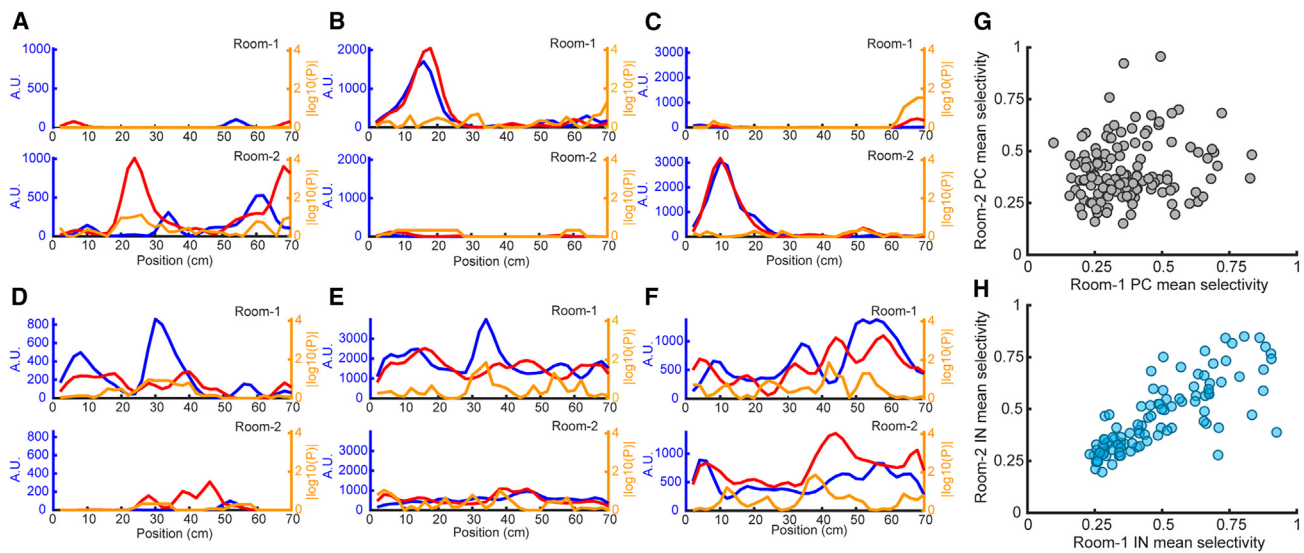
Figure 6. Remapping of context selectivity in a novel environment
(A) Both place field and splitter field are present only in the second environment (room 2).
(B) Both place field and splitter field disappear in the second environment.
(C) Only place field, without splitter feature, emerged in the second environment.
(D) Mixed-effect neuron.
(A–D) Pyramidal cells. Right axis, p values (dissimilarity).
(E) An interneuron that loses selectivity in room 2.
(F) Interneuron with rearranged context selectivity.
(G and H) Remapping of context-selective activity of (G) pyramidal cells and (H) interneurons in delay sessions represented by plotting selectivity in a familiar versus in a novel room (interneurons: R = 0.83, p < 0.0001; pyramidal cells: R = 0.12, p = 0.16).

population level, the SI of interneurons showed a negative correlation with the proportion of their monosynaptically connected pyramidal neuron partners (Figure 5J). This finding indicates that interneurons integrate spikes from many upstream pyramidal neurons and that their particular choice-correlated features are derived from their non-uniform P-I connections.

"Remapping" of choice-predicting activity in novel environment

An important feature of place fields of pyramidal cells is that their spatial relationships are different across different environments.[27,38] Therefore, we examined whether splitter fields also show such remapping.[38] Three mice in the delayed group were tested in a novel room after completing test runs in the familiar figure-8 maze. Examples of remapping place cells and interneurons are shown in Figures 6A–6F. The prevalence of splitter fields was slightly higher in the novel compared to the familiar environment. Importantly, SI tuning curves of pyramidal neurons were significantly decorrelated across the two environments (Figure 6G), indicating the remapping of splitter properties. In contrast, we found a strong correlation between tuning curves of interneurons across the two environments (Figure 6H), that is, splitter feature was interneuron specific, in contrast to pyramidal cells.

The role of medial entorhinal cortex (mEC) in choice prediction properties of hippocampal neurons

Splitter features of hippocampal neurons can be induced locally or inherited from upstream regions.[25] To examine the role of up-

stream inputs to the hippocampus on splitter features, we reanalyzed a published dataset.[27] In addition to recording from CA1 neurons, these mice were also implanted with ipsilateral (n = 18) or bilateral (n = 3) optic fibers in the mEC to optogenetically activate all types of GABAergic interneurons (by AAV5-mDlx-ChR2-mCherry virus) and thus silence mEC output (Figures 7A and 7B). The fraction of pyramidal neurons with place fields on the center arm was only slightly reduced by the bilateral manipulation; therefore, a sufficient number of fields persisted to perform splitter cell analyses. Because bilateral manipulations led to remapping,[27] place fields were defined separately for no-stimulation and stimulation trials. Ipsilateral silencing of the mEC did not significantly affect the fraction of splitter neurons, defined by a modified version of the dissimilarity index (i.e., significant [p < 0.05] difference in the within-field average left versus right firing rates using Wilcoxon rank-sum test). However, during bilateral mEC inactivation, the fraction of splitter fields decreased significantly (Figures 7B–7D), implying that the mEC or circuits upstream of it may be important for the context-specific firing of hippocampal neurons.

DISCUSSION

We found that task-context (splitter) feature of hippocampal pyramidal neurons is a continuum and highly variable along both trial and position axes and that the distinction between classic place and splitter fields depends on experimenter-biased arbitrary criteria and experimental conditions. Splitter features of
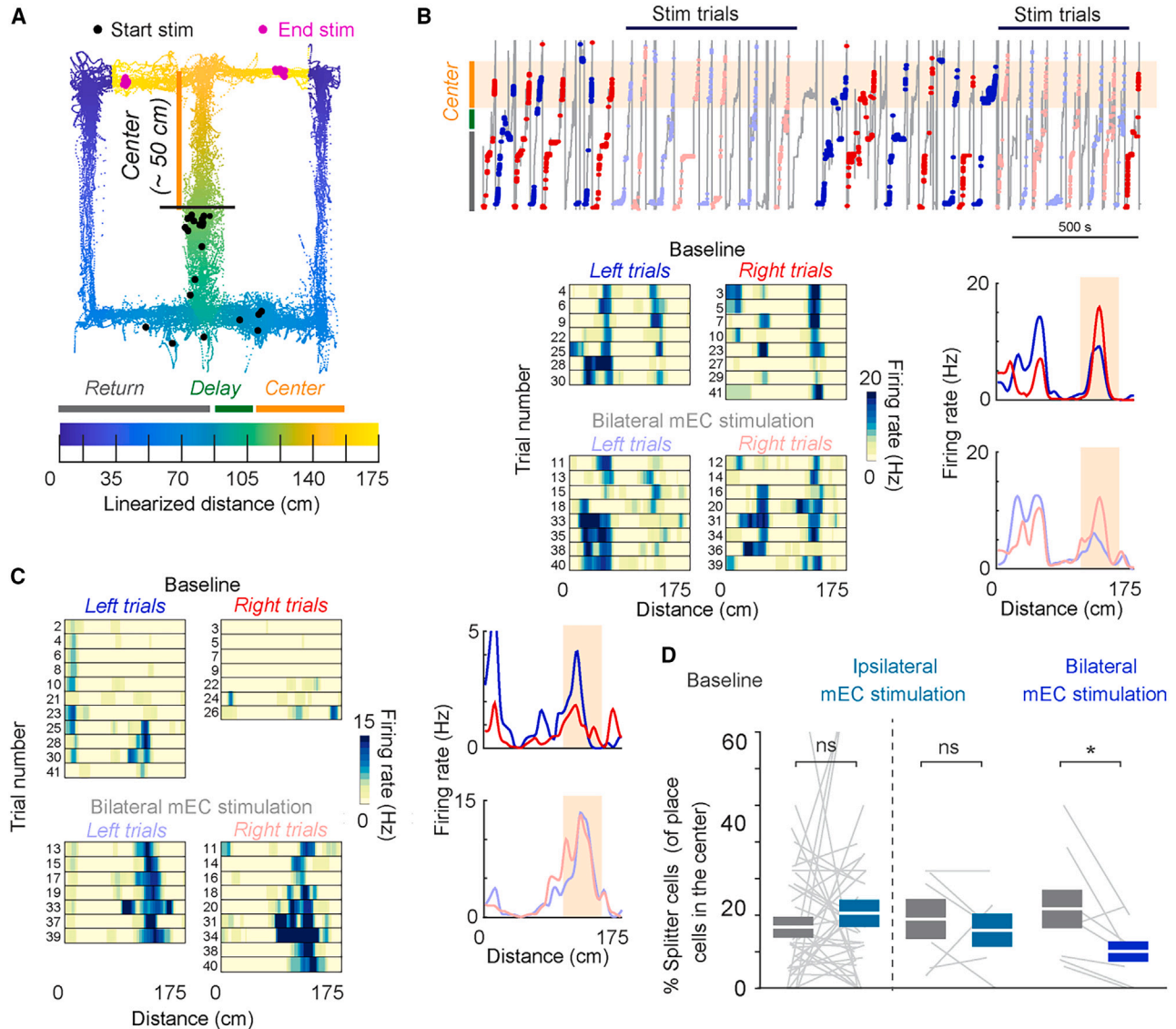
Figure 7. Bilateral, but not ipsilateral, mEC silencing decreased the fraction of CA1 splitter cells

(A) Travel trajectory of the mouse in an example session, superimposed on the figure-8 maze. Square pulse stimulation was targeted in blocks of 10 trials to the center arm of the track, turning on at door opening (black horizontal line) at the end of a 10-s delay between trials. The mouse's position at the start of stimulation across trials is shown as black dots. Stimulation stopped once the mouse crossed an infrared detector located after the mouse made a choice (magenta dots). The maze was linearized according to the colormap as shown. Analysis was restricted to cells with a field in the "center zone" (yellow line).

(B) Top: linearized trajectory in gray, with spikes from a single neuron overlaid as dots. Blue and red dots: leftward and rightward baseline trials, respectively. Light blue and light red: leftward and rightward trials during bilateral mEC stimulation, respectively. The shaded box in the background shows the center zone. Bottom left: trial-by-trial rate maps for the same cell. Bottom right: across-trial averages for the same cell. To classify cells as splitter, the average firing across trials was tested for significance between left and right trajectories (Wilcoxon rank-sum test). This cell was significantly splitting during both baseline and stimulation conditions.

(C) Same as (B) but for a different cell. During mEC inactivation, the cell formed a new place field in the center zone (after trial 11) that did not distinguish between left and right trajectories. Note that the new field persisted during subsequent baseline trials, where it discriminated between left and right trajectories.

(D) Percentage of neurons with significant left versus right firing rate differences (splitter cells) during each manipulation out of all defined PCs on the center arm. Left of dashed line: ipsilateral silencing results from the cohort of 18 mice with ipsilateral targeting only. Gray: control trials, light blue: ipsilateral mEC silencing (n = 46 sessions from 18 mice, Wilcoxon signed rank test, Z = −0.34, p = 0.7355). Right of dashed line: results from the cohort of 3 mice with bilateral mEC silencing. Gray: control trials, light blue: ipsilateral mEC silencing, dark blue: bilateral silencing of the entorhinal cortex (Wilcoxon signed rank test, ipsilateral mEC, n = 6 sessions from 3 mice, p = 0.8125; bilateral mEC, n = 9 sessions from 3 mice, p = 0.0234). *p < 0.05. Boxplots indicate mean ± SEM. Numbers of center arm place fields/total pyramidal cells in the bilateral mice dataset (n = 3) were as follows: baseline, 116/326; during ipsilateral mEC inactivation, 92/326; during bilateral baseline, 162/453; and bilateral mEC inactivation, 100/453. In the ipsilaterally implanted mouse dataset (18 mice), the numbers were baseline, 686/1,874 and ipsilateral inactivation mEC, 632/1,874.

neurons can be identified by either firing rate differences or spatial offsets of neuronal activity, and these features can remap across testing situations. Even typical place fields can be differentiated into subfields by the behavioral choice of the animal, and splitting subfields can evolve within a single place field. Neurons can acquire or lose splitter features across trials even when place field features remain unaltered. Two place fields from the same neuron can individually encode both past or future run trajectories, implying that splitter fields are under the control of assembly activity. Splitter field populations initially express retrospective (past choice) features, which gradually evolve to prospective (future choice) features along the central arm of the maze. A fraction of interneurons can also differentiate left and right choices by integrating inputs from their partner pyramidal cells. Finally, we demonstrated that bilateral optogenetic inactivation of the mEC reversibly decreased the fraction of splitter fields. Overall, our findings suggest that (1) hippocampal neurons are activated in ensembles, which can combine both past and future-predicting experiences influenced by the currently perceived environment, and (2) place or splitter features are different manifestations of the same hippocampal computation.

Continuum of place fields and splitter fields

Previous studies have already pointed out that the fraction of splitter fields and variability across studies not only depends on experimenter-imposed arbitrary thresholds but also by experimental design.[3] In addition to confirming that in a delayed version of the same spatial alternation task, fewer neurons were identifiable as splitters than in the continuous version,[5] we found that several aspects of the neuronal computation differed in the two tasks. Mean selectivity was higher, and the proportion of trials with a match between correct/erroneous arm choices and splitter cell firing patterns was larger. The fraction of splitter fields increased from start to end in the central arm, and this fraction was also higher in the continuous than in the delayed task. Furthermore, the correlation between selectivity and left versus right tuning curve difference was higher in the continuous task. The SI more strongly predicted the choice outcome, and neurons with double place fields displayed mainly opposite arm choices in the continuous task but not in its delayed version. The population firing rate vectors also predicted future choices better in the continuous than in the delayed task. In the continuous task, a high selectivity characterized more than half of the population, and almost every place field had some degree of context selectivity. In contrast, the highest incidence of splitter features in the delayed task was observed in the delay area, prior to the mouse's entry into the central arm, corroborating an earlier finding.[5] The movement trajectories of the animal's paths were also characteristically different in the two tasks, especially in the early part of the central arm. Thus, just a 5-s delay demand on working memory exerted a large impact at multiple levels of neuronal organization. This implies that hippocampal computation becomes more demanding when delay is required between choices.

Besides working memory load, experience also influences splitter activity.[14,39] These findings imply that well-trained animals represent both central and side arms together as one context separate from the opposite trial, the other context, irrespective of the overlapping stem segment. Interestingly, the slope of regression between error rate and prevalence of splitter activity was steeper in continuous compared to delay sessions. Thus, insertion of delay in a trajectory not only puts pressure on working memory but also interferes with the representation of a trial as one context.

Making choices with splitter cells

What mechanisms are responsible for the conspicuous firing pattern differences in the continuous versus delayed version of this working memory task? Comparison with previous experiments with longer delays may provide clues. When rats were required to run continuously in a wheel for 15–20 s during the delay, splitter cell populations persisted throughout the run.[24,40,41] However, the largest fraction of neurons with side predicting features was present in the first second of the run, decaying rapidly with time. This rapidly decreasing fractional change occurred in parallel with the increasing duration ("time field") and size of the firing fields of the neurons from the beginning to the end of the delay.[24] Subsequent analysis of "time cells"[41–46] during forced running on a treadmill revealed that their progressively expanding time fields could be described quantitatively by the logarithmic Weber-Fechner law.[47] The logarithmic rule predicts a precisely linear relationship between within-trial time-field width and elapsed time. Thus, the same logarithmic rule seems to describe the temporal evolution of the fraction of splitter cells and the duration and size (i.e., distance) of place fields, suggesting that the same underlying physiological mechanisms are responsible for the evolving firing patterns during working memory.

For practical reasons, splitter fields are typically reported in the central arm of the maze,[6,7] where external factors can be discounted. But memory (splitter) features of pyramidal cells are expected to arise prior to the animal's entering the delay area or central arm. The likely time point of initiating a new neuronal trajectory is consumption of the reward ("evidence maximum"), an act which verifies the correctness of the previous choice. We hypothesize that the reward creates an affordance for a change in brain state from the theta oscillations to the emergence of sharp wave ripples.[48] This shift can trigger a new initial condition.[42] From this new seed, another neuronal trajectory evolves from the reward area through the delay box, the central arm, and the side arm of the maze until the next reward is reached. The hypothesis of evolving unique neuronal trajectories can explain the large and small fractions of splitter fields in continuous and delayed tasks, respectively. Because of the logarithmic decay rule, the fraction of future-choice-predicting neurons rapidly decreases after the reward is consumed and the new neuronal trajectory is launched. By the time the animal enters the central arm in the delayed version of the task, the fraction of choice-predicting neurons has already decreased substantially.[24]

The logarithmic decay rule has implications about choices and route execution in the maze. The highest "confidence" about the future choice in the brain is present immediately after the reward-induced brain state change, and the confidence level, as measured by the fraction of splitter fields, decreases rapidly to a low level by the time the animal arrives to the T junction of the maze (often referred to as a "choice point"). Yet, the choice

is "made" in the side arm immediately after the reward rather than at the T junction. This hypothesis is supported by the behavioral observation that the animal's run from start to reward is a smooth ("ballistic") trajectory and that trained animals rarely stop and pause at the postulated choice point.

Splitter cells in the hippocampus and other brain regions

Neurons with splitter features have been described in multiple brain regions outside the hippocampus, including the entorhinal cortex,[7] the prefrontal cortex[25,49] and the nucleus reuniens of the thalamus.[25] It has been suggested that a prefrontal-thalamic neural circuit is essential for hippocampal representation of routes or trajectories through the environment. Lesioning or optogenetic silencing of the nucleus reuniens substantially reduced the fraction of splitter cells in the hippocampal CA1 neurons, suggesting that goals are computed in the prefrontal cortex and transferred to the hippocampus via the direct nucleus reuniens-CA1 path.[25] Our findings expand and somewhat modify this suggestion. While ipsilateral silencing of the mEC barely affected the fraction of splitter fields, bilateral inactivation reduced their fraction several-fold. This decrease was larger than the fraction of place field decrease,[27] suggesting that the entorhinal cortex is also important for the selection of the future path. This conclusion is supported by the similar fraction of splitter cells present in the CA1, CA3, and dentate regions[50] because neurons of nucleus reuniens project only to the CA1 region[51] and thus are not expected to influence the upstream CA3 and dentate neurons. From these observations, one can assume that the hippocampus and its partner structures interact with each other and "decide" the form of the ensuing trajectory immediately after the reward-afforded brain state change. Thus, the future path (choice) is dictated by the past path (memory).

Splitter features of interneurons

Fast-firing interneurons often show position-specific firing rate changes and theta spike phase precession within their firing fields. These features may be inherited from their monosynaptically connected pyramidal cells.[35–37] Inheritance can also explain the splitter features of interneurons. If each interneuron received equal strength input from many pyramidal cells, then one would expect a flat tuning curve along the entire maze during both left and right trials. However, input strengths to interneurons from their upstream pyramidal neurons are highly skewed,[37] resulting in a biased control of interneuron firing. Interneurons with fewer pyramidal cell partners are expected to have stronger bias per pyramidal cell and thus accentuated selectivity, and this is what we observed. Interneurons with fewer detected presynaptic pyramidal neurons had higher choice selectivity than interneurons with many pyramidal cell partners.

Interneurons preserved their magnitude of SI across different environments, in contrast to the orthogonal distribution of selectivity features of pyramidal neurons. This difference can be also explained by the skewed anatomical connectivity structure. We hypothesize that interneurons with fewer pyramidal partners were under the guidance of different pyramidal cells in the two environments (because pyramidal cells remapped) but that each small assembly exerted a stronger control on them compared to interneurons, which were innervated by large numbers of pyramidal cells.

Limitations of the study

Some conceptual and technical caveats should be mentioned. While the idea that the abstract cognitive map guides navigation is a general assumption, how activity of goal-correlated neurons is transduced to actual footsteps needed for the animal to reach its goal has no clear mechanism. If splitter neurons arise in the prefrontal cortex and are transferred serially to the nucleus reuniens, entorhinal cortex, and hippocampus/subiculum, then the nature of the downstream actuator still remains to be discovered. The activity of goal-directed hippocampal output may affect deep layers of the entorhinal cortex, which in turn spreads it to wide areas of the neocortex. Alternatively, the motor actuator can be the lateral septum and the hypothalamus. In contrast to such a serial route, it is also possible that the prefrontal cortex itself can inform motor structures directly, yet it sends a corollary return signal to the hippocampus for coordinating egocentric goals and allocentric spatial maps. Our correlational results cannot make these distinctions.

We found that a subset of interneurons also displayed splitter features and assumed that they inherited them from their monosynaptically connected pyramidal cells. However, we do not have a reliable physiological measure of the interneuron-pyramidal inhibitory connection; thus, the possibility remains that interneurons play a more active role in the generation of splitter cells than discussed in our paper. Furthermore, the molecular identity of the splitter interneurons (i.e., their types) could not be revealed in the current study.

Finally, we conjectured that a unique splitter trajectory is initiated after the reward, but we did not demonstrate the existence of splitter neurons or population vector in the return arm leading to the delay area. A comparison of firing patterns in the return arm in correct trials and in opposite arm-choice error trials will be needed in future experiments to address this caveat.

STAR★METHODS

Detailed methods are provided in the online version of this paper and include the following:

- KEY RESOURCES TABLE
- RESOURCE AVAILABILITY
  - Lead contact
  - Materials availability
  - Data and code availability
- EXPERIMENTAL MODEL AND SUBJECT PARTICIPANT DETAILS
  - Datasets
  - Animals
- METHOD DETAILS
  - Behavioral training
  - Surgery
  - Recording of hippocampal activity
  - Spike sorting
  - Neuron classification
  - Calculation of tuning curves

- ○ Identification of place fields
- ○ Quantification of context-correlated activity
- ○ Clustering of place fields based on Selectivity and Dissimilarity
- ○ Retrospective – Prospective bias of neuronal activity
- ○ Analysis of past/future-correlated population activity
- ○ Identification of place cell assemblies
- ○ Position estimation by template matching
- ○ Identification of putative monosynaptic connections
- ○ Prediction of interneuron spiking by activity of place cells
- ● QUANTIFICATION AND STATISTICAL ANALYSIS

AUTHOR CONTRIBUTIONS

V.V. and G.B. conceived and designed the experiments; V.V., I.Z., Y.Z., and R.H. performed all experiments; V.V., P.P., and I.Z. analyzed data; and G.B. and V.V. wrote the manuscript with contributions from the other authors.

DECLARATION OF INTERESTS

The authors declare no competing interests.

REFERENCES

1. O'Keefe, J., and Nadel, L. (1978). The hippocampus as a Cognitive Map (Clarendon Press).

2. McNaughton, B.L., Barnes, C.A., and O'Keefe, J. (1983). The contributions of position, direction, and velocity to single unit activity in the hippocampus of freely-moving rats. Exp. Brain Res. 52, 41–49. https://doi.org/10.1007/BF00237147.

3. Duvelle, É., Grieves, R.M., and van der Meer, M.A.A. (2023). Temporal context and latent state inference in the hippocampal splitter signal. Elife 12, e82357. https://doi.org/10.7554/eLife.82357.

4. Hasselmo, M.E., and Eichenbaum, H. (2005). Hippocampal mechanisms for the context-dependent retrieval of episodes. Neural Netw. 18, 1172–1190. https://doi.org/10.1016/j.neunet.2005.08.007.

5. Ainge, J.A., Van Der Meer, M.A.A., Langston, R.F., and Wood, E.R. (2007). Exploring the role of context-dependent hippocampal activity in spatial alternation behavior. Hippocampus 17, 988–1002. https://doi.org/10.1002/hipo.20301.

6. Wood, E.R., Dudchenko, P.A., Jonathan Robitsek, R., and Eichenbaum, H. (2000). Hippocampal Neurons Encode Information about Different Types of Memory Episodes Occurring in the Same Location. Neuron 27, 623–633. https://doi.org/10.1016/s0896-6273(00)00071-4.

7. Frank, L.M., Brown, E.N., and Wilson, M. (2000). Trajectory Encoding in the Hippocampus and Entorhinal Cortex. Neuron 27, 169–178. https://doi.org/10.1016/s0896-6273(00)00018-0.

8. D. Derdikman and J.J. Knierim, eds. (2014). Space,Time and Memory in the Hippocampal Formation (Springer Vienna). https://doi.org/10.1007/978-3-7091-1292-2.

9. Ferbinteanu, J., and Shapiro, M.L. (2003). Prospective and Retrospective Memory Coding in the Hippocampus. Neuron 40, 1227–1239. https://doi.org/10.1016/s0896-6273(03)00752-9.

10. Eichenbaum, H. (2017). On the Integration of Space, Time, and Memory. Neuron 95, 1007–1018. https://doi.org/10.1016/j.neuron.2017.06.036.

11. Wikenheiser, A.M., and Redish, A.D. (2015). Decoding the cognitive map: Ensemble hippocampal sequences and decision making. Curr. Opin. Neurobiol. 32, 8–15. https://doi.org/10.1016/j.conb.2014.10.002.

12. Dudchenko, P.A., and Wood, E.R. (2015). Place fields and the cognitive map. Hippocampus 25, 709–712. https://doi.org/10.1002/hipo.22450.

13. Kinsky, N.R., Mau, W., Sullivan, D.W., Levy, S.J., Ruesch, E.A., and Hasselmo, M.E. (2020). Trajectory-modulated hippocampal neurons persist throughout memory-guided navigation. Nat. Commun. 11, 2443. https://doi.org/10.1038/s41467-020-16226-4.

14. Levy, S.J., Kinsky, N.R., Mau, W., Sullivan, D.W., and Hasselmo, M.E. (2021). Hippocampal spatial memory representations in mice are heterogeneously stable. Hippocampus 31, 244–260. https://doi.org/10.1002/hipo.23272.

15. Zhao, X., Hsu, C.L., and Spruston, N. (2022). Rapid synaptic plasticity contributes to a learned conjunctive code of position and choice-related information in the hippocampus. Neuron 110, 96–108. https://doi.org/10.1016/j.neuron.2021.10.003.

16. Harvey, R.E., Robinson, H.L., Liu, C., Oliva, A., and Fernandez-Ruiz, A. (2023). Hippocampo-cortical circuits for selective memory encoding, routing, and replay. Neuron 111, 2076–2090.e9. https://doi.org/10.1016/j.neuron.2023.04.015.

17. Ainge, J.A., Dudchenko, P.A., and Wood, E.R. (2008). Context-Dependent Firing of Hippocampal Place Cells: Does It Underlie Memory? In Hippocampal Place Fields (Oxford University Press), pp. 44–58. https://doi.org/10.1093/acprof:oso/9780195323245.003.0004.

18. Dayawansa, S., Kobayashi, T., Hori, E., Umeno, K., Tazumi, T., Ono, T., and Nishijo, H. (2006). Conjunctive effects of reward and behavioral episodes on hippocampal place-differential neurons of rats on a mobile treadmill. Hippocampus 16, 586–595. https://doi.org/10.1002/hipo.20186.

19. Bahar, A.S., and Shapiro, M.L. (2012). Remembering to learn: Independent place and journey coding mechanisms contribute to memory transfer. J. Neurosci. 32, 2191–2203. https://doi.org/10.1523/JNEUROSCI.3998-11.2012.

20. Ferbinteanu, J., Shirvalkar, P., and Shapiro, M.L. (2011). Memory modulates journey-dependent coding in the rat hippocampus. J. Neurosci. 31, 9135–9146. https://doi.org/10.1523/JNEUROSCI.1241-11.2011.

21. Takahashi, S. (2013). Hierarchical organization of context in the hippocampal episodic code. Elife 2, e00321. https://doi.org/10.7554/eLife.00321.

22. Miller, K.J., Botvinick, M.M., and Brody, C.D. (2017). Dorsal hippocampus contributes to model-based planning. Nat. Neurosci. 20, 1269–1276. https://doi.org/10.1038/nn.4613.

23. Berke, J.D., Breck, J.T., and Eichenbaum, H. (2009). Striatal versus hippocampal representations during win-stay maze performance. J. Neurophysiol. 101, 1575–1587. https://doi.org/10.1152/jn.91106.2008.

24. Pastalkova, E., Itskov, V., Amarasingham, A., and Buzsáki, G. (2008). Internally generated cell assembly sequences in the rat hippocampus. Science 321, 1322–1327. https://doi.org/10.1126/science.1159775.

25. Ito, H.T., Zhang, S.J., Witter, M.P., Moser, E.I., and Moser, M.B. (2015). A prefrontal-thalamo-hippocampal circuit for goal-directed spatial navigation. Nature *522*, 50–55. https://doi.org/10.1038/nature14396.

26. O'Keefe, J., and Krupic, J. (2021). Do hippocampal pyramidal cells respond to nonspatial stimuli? Physiol. Rev. *101*, 1427–1456. https://doi.org/10.1152/physrev.00014.2020.

27. Zutshi, I., Valero, M., Fernández-Ruiz, A., and Buzsáki, G. (2022). Extrinsic control and intrinsic computation in the hippocampal CA1 circuit. Neuron *110*, 658–673.e5. https://doi.org/10.1016/j.neuron.2021.11.015.

28. Petersen, P.C., Siegle, J.H., Steinmetz, N.A., Mahallati, S., and Buzsáki, G. (2021). CellExplorer: A framework for visualizing and characterizing single neurons. Neuron *109*, 3594–3608. https://doi.org/10.1016/j.neuron.2021.09.002.

29. Barth, A.M., Domonkos, A., Fernandez-Ruiz, A., Freund, T.F., and Varga, V. (2018). Hippocampal Network Dynamics during Rearing Episodes. Cell Rep. *23*, 1706–1715. https://doi.org/10.1016/j.celrep.2018.04.021.

30. Prerau, M.J., Lipton, P.A., Eichenbaum, H.B., and Eden, U.T. (2014). Characterizing context-dependent differential firing activity in the hippocampus and entorhinal cortex. Hippocampus *24*, 476–492. https://doi.org/10.1002/hipo.22243.

31. Maurer, A.P., Cowen, S.L., Burke, S.N., Barnes, C.A., and McNaughton, B.L. (2006). Organization of hippocampal cell assemblies based on theta phase precession. Hippocampus *16*, 785–794. https://doi.org/10.1002/hipo.20202.

32. Zhang, K., Ginzburg, I., McNaughton, B.L., and Sejnowski, T.J. (1998). Interpreting neuronal population activity by reconstruction: unified framework with application to hippocampal place cells. J. Neurophysiol. *79*, 1017–1044. https://doi.org/10.1152/jn.1998.79.2.1017.

33. Lopes-dos-Santos, V., Ribeiro, S., and Tort, A.B.L. (2013). Detecting cell assemblies in large neuronal populations. J. Neurosci. Methods *220*, 149–166. https://doi.org/10.1016/j.jneumeth.2013.04.010.

34. Geisler, C., Robbe, D., Zugaro, M., Sirota, A., and Buzsáki, G. (2007). Hippocampal place cell assemblies are speed-controlled oscillators. Proc Natl Acad Sci USA *104*, 8149–8154. https://doi.org/10.1073/pnas.0610121104.

35. Marshall, L., Henze, D.A., Hirase, H., Leinekugel, X., Dragoi, G., and Buzsáki, G. (2002). Hippocampal Pyramidal Cell-Interneuron Spike Transmission Is Frequency Dependent and Responsible for Place Modulation of Interneuron Discharge. J. Neurosci. *22*, RC197. https://doi.org/10.1523/JNEUROSCI.22-02-j0001.2002.

36. Maurer, A.P., Cowen, S.L., Burke, S.N., Barnes, C.A., and McNaughton, B.L. (2006). Phase precession in hippocampal interneurons showing strong functional coupling to individual pyramidal cells. J. Neurosci. *26*, 13485–13492. https://doi.org/10.1523/JNEUROSCI.2882-06.2006.

37. English, D.F., McKenzie, S., Evans, T., Kim, K., Yoon, E., and Buzsáki, G. (2017). Pyramidal Cell-Interneuron Circuit Architecture and Dynamics in Hippocampal Networks. Neuron *96*, 505–520.e7. https://doi.org/10.1016/j.neuron.2017.09.033.

38. Kubie, J.L., Levy, E.R.J., and Fenton, A.A. (2020). Is hippocampal remapping the physiological basis for context? Hippocampus *30*, 851–864. https://doi.org/10.1002/hipo.23160.

39. Smith, D.M., and Mizumori, S.J.Y. (2006). Learning-related development of context-specific neuronal responses to places and events: the hippocampal role in context processing. J. Neurosci. *26*, 3154–3163. https://doi.org/10.1523/JNEUROSCI.3234-05.2006.

40. Gill, P.R., Mizumori, S.J.Y., and Smith, D.M. (2011). Hippocampal episode fields develop with learning. Hippocampus *21*, 1240–1249. https://doi.org/10.1002/hipo.20832.

41. MacDonald, C.J., Lepage, K.Q., Eden, U.T., and Eichenbaum, H. (2011). Hippocampal "time cells" bridge the gap in memory for discontiguous events. Neuron *71*, 737–749. https://doi.org/10.1016/j.neuron.2011.07.012.

42. Itskov, V., Curto, C., Pastalkova, E., and Buzsáki, G. (2011). Cell assembly sequences arising from spike threshold adaptation keep track of time in the hippocampus. J. Neurosci. *31*, 2828–2834. https://doi.org/10.1523/JNEUROSCI.3773-10.2011.

43. Kraus, B.J., Robinson, R.J., White, J.A., Eichenbaum, H., and Hasselmo, M.E. (2013). Hippocampal "Time Cells": Time versus Path Integration. Neuron *78*, 1090–1101. https://doi.org/10.1016/j.neuron.2013.04.015.

44. Mau, W., Sullivan, D.W., Kinsky, N.R., Hasselmo, M.E., Howard, M.W., and Eichenbaum, H. (2018). The Same Hippocampal CA1 Population Simultaneously Codes Temporal Information over Multiple Timescales. Curr. Biol. *28*, 1499–1508. https://doi.org/10.1016/j.cub.2018.03.051.

45. Taxidis, J., Pnevmatikakis, E.A., Dorian, C.C., Mylavarapu, A.L., Arora, J.S., Samadian, K.D., Hoffberg, E.A., and Golshani, P. (2020). Differential Emergence and Stability of Sensory and Temporal Representations in Context-Specific Hippocampal Sequences. Neuron *108*, 984–998. https://doi.org/10.1016/j.neuron.2020.08.028.

46. Eichenbaum, H. (2014). Time cells in the hippocampus: a new dimension for mapping memories. Nat. Rev. Neurosci. *15*, 732–744. https://doi.org/10.1038/nrn3827.

47. Cao, R., Bladon, J.H., Charczynski, S.J., Hasselmo, M.E., and Howard, M.W. (2022). Internally Generated Time in the Rodent Hippocampus is Logarithmically Compressed. Elife *11*, e75353. https://doi.org/10.7554/eLife.75353.

48. Buzsáki, G. (1989). Two-stage model of memory trace formation: A role for "noisy" brain states. Neuroscience *31*, 551–570. https://doi.org/10.1016/0306-4522(89)90423-5.

49. Fujisawa, S., Amarasingham, A., Harrison, M.T., and Buzsáki, G. (2008). Behavior-dependent short-term assembly dynamics in the medial prefrontal cortex. Nat. Neurosci. *11*, 823–833. https://doi.org/10.1038/nn.2134.

50. Senzai, Y., and Buzsáki, G. (2017). Physiological Properties and Behavioral Correlates of Hippocampal Granule Cells and Mossy Cells. Neuron *93*, 691–704.e5. https://doi.org/10.1016/j.neuron.2016.12.011.

51. Herkenham, M. (1978). The connections of the nucleus reuniens thalami: evidence for a direct thalamo-hippocampal pathway in the rat. J. Comp. Neurol. *177*, 589–610. https://doi.org/10.1002/cne.901770405.

52. Huszár, R., Zhang, Y., Blockus, H., and Buzsáki, G. (2022). Preconfigured dynamics in the hippocampus are guided by embryonic birthdate and rate of neurogenesis. Nat. Neurosci. *25*, 1201–1212. https://doi.org/10.1038/s41593-022-01138-x.

53. Cao, L., Varga, V., and Chen, Z.S. (2021). Uncovering spatial representations from spatiotemporal patterns of rodent hippocampal field potentials. Cell Rep. Methods *1*, 100101. https://doi.org/10.1016/j.crmeth.2021.100101.

54. Vandecasteele, M., Varga, V., Berényi, A., Papp, E., Barthó, P., Venance, L., Freund, T.F., and Buzsáki, G. (2014). Optogenetic activation of septal cholinergic neurons suppresses sharp wave ripples and enhances theta oscillations in the hippocampus. Proc. Natl. Acad. Sci. USA *111*, 13535–13540. https://doi.org/10.1073/pnas.1411233111.

55. Vandecasteele, M., M.S., Royer, S., Belluscio, M., Berényi, A., Diba, K., Fujisawa, S., Grosmark, A., Mao, D., Mizuseki, K., et al. (2012). Large-scale recording of neurons by movable silicon probes in behaving rodents. J. Vis. Exp., e3568. https://doi.org/10.3791/3568.

56. Vöröslakos, M., Miyawaki, H., Royer, S., Diba, K., Yoon, E., Petersen, P.C., and Buzsáki, G. (2021). 3d-printed recoverable microdrive and base plate system for rodent electrophysiology. Bio. Protoc. *11*, e4137. https://doi.org/10.21769/BioProtoc.4137.

57. Pachitariu, M., Steinmetz, N., Kadir, S., Carandini, M., and Harris, K. (2016). Fast and accurate spike sorting of high-channel count probes with KiloSort. NeurIPS Proceedings *29*.

STAR★METHODS

KEY RESOURCES TABLE

REAGENT or RESOURCE	SOURCE	IDENTIFIER
Bacterial and virus strains		
AAV5-hSyn-hChR2(H134R)-EYFP	UNC Vector Core	N/A
AAV5-mDlx-ChR2-mCherry	Plasmid gift from Dr. Gord Fishell, Virus custom prepared by Addgene	N/A
Chemicals, peptides, and recombinant proteins		
Paladur cold-curing acrylic (liquid + powder)	Kulzer International	Art#:64707937 Art#:64707945
Optibond Universal dental adhesive bottle kit	Kerr	Art#:36517
Experimental models: Organisms/strains		
C57BL/6NCrl	Charles River	IMSR_CRL:027
C57BL/6-Tg(Grik4-cre)G32-4Stl/J	The Jackson Laboratory	IMSR_JAX:006474
Recombinant DNA		
pAAV-CaMKIIa-hChR2(H134R)-EYFP	Addgene	Plasmid #26969
pCAG-tdTomato	Addgene	Plasmid #83029
Software and algorithms		
MATLAB (versions: R2018b, R2021a, 2022b, 2023a, 2023b)	Mathworks Inc	SCR_001622
Phy (Python GUI for manual spike curation)	Cyrille Rossant, Ken Harris et al.	https://github.com/cortex-lab/phy
Python 3.5	python.org	SCR_008394
Kilosort (template based spike sorting MATLAB software)	Pachitariu M & Cortex-lab	https://github.com/cortex-lab/KiloSort
CellExplorer (Cell classification pipeline and graphical interface)	Petersen et al., 2020	https://linkinghub.elsevier.com/retrieve/pii/S0896627321006565
Custom MATLAB scripts	Viktor Varga	https://doi.org/10.5281/zenodo.10277331
Other		
Silicon probes	Neuronexus, Cambridge Neurotech, Diagnostic Biochips (DBC)	A2x32-Poly5-10mm-20s-200-100-H64LP_30mm; A4x16-5mm-50-500-703-H64LP_30mm; Buzsaki64_5x12-H64LP_30mm; A4x16- Poly2-5mm-20s-150-160-H64LP_30mm; A5x12-16-Buz-Lin-5mm-100-200-160-177-H64LP_30mm; Cambridge NeuroTech, H2 (64 ch); Cambridge NeuroTech, H3 (64 ch); DBC P64-1-D; DBC P128-2;
RHD2000 USB Interface Board	Intan Technologies	C3100
64 channel digital amplifies	Intan Technologies	C3314

RESOURCE AVAILABILITY

Lead contact

Further information and requests for resources should be directed to and will be fulfilled by the lead contact, György Buzsáki (gyorgy.buzsaki@nyulangone.org).

Materials availability
This study did not generate new unique reagents.

Data and code availability
- All the data of this study is publicly available in the Buzsáki Lab Databank: https://buzsakilab.com/wp/public-data/.
- All custom code for preprocessing the data is freely available on the Buzsáki Laboratory repository: https://github.com/buzsakilab/buzcode, and scripts specific for analyzing these datasets can be found on Zenodo: https://zenodo.org/records/10277331.
- Any additional information required to reanalyze the data reported in this paper is available from the lead contact upon request.

EXPERIMENTAL MODEL AND SUBJECT PARTICIPANT DETAILS

Datasets
This study is based on the analysis of three datasets, certain aspects of them already published. Therefore, details about animals, virus injections, surgical procedures, behavioral tests and recording can be found in the respective publications.[27,52,53] Besides the aforementioned publications, extensive description of all experiments used in this study can be found in the Buzsaki lab database (https://buzsakilab.com/wp/projects/entry/67125/, [28];). Hence, all procedures not relevant for this study will only be briefly mentioned here.

Animals
Only male mice were used in this study. To our knowledge, the explored phenomena are not sex-specific therefore, our findings are expected to be valid in female subjects as well.

Dataset1
Five wild type male adult (age: P60 – P120, weight: 25–29 g) mice from the C57BL6 strain were used for this project. Mice were purchased from Charles River Laboratory and were housed in the animal facility of NYU Langone Health's Neuroscience Institute. An AAV5.hSyn.ChR2(H134R).EYFP (UNC Vector Core) viral construct was injected into the medial septum of these mice. For this study only control sessions without light stimulation were used or in case of one animal light was delivered outside the skull (sham stimulation). In yet another mouse virally transduced axons could not be detected histologically in the dorsal hippocampus and all sessions in this mouse were used for the current manuscript (basic information about animals and sessions used in this study can be found in Table S1 and all further details can be looked up in the Buzsaki lab database).

Dataset2
C57BL6 adult mice (age: P90-P180, weight: 24g–30g) from Charles River Laboratory were used in the delayed alternation task (n = 4). Animals underwent *in utero* electroporation of the pAAV-CaMKIIa-hChR2(H134R)-EYFP and pCAG-tdTomato plasmids for birthdating their hippocampal pyramidal neurons for another study (see[54]).

Dataset3
For the mEC silencing dataset, 3 heterozygous Grik4-cre male mice (Jackson Labs, Stock No: 006474) were used for bilateral silencing while an additional 15 Grik4-cre male mice were used for unilateral silencing (age: P120-P300, weight: 22g–39g). An AAV5-mDlx-ChR2-mCherry viral construct was injected either unilaterally or bilaterally into the mEC with optic fiber implants (200 μm) over each injection site. Detailed methods can be found in.[27]

All experiments) were approved by the Institutional Animal Care and Use Committee at the New York University Langone Health (protocol ID: s1501466). All mice were kept in the vivarium on a 12-hout light/dark cycle and were housed in groups of 2–3 per cage before surgery. Following probe implantation, mice were housed separately. Prior to behavior training, animals were provided (Datasets 1–3) water and food *ad libitum*. During behavioral training water access was restricted to 1 mL/day. If mice's weight had dropped below 85% of pre-restriction, water restriction was terminated.

METHOD DETAILS

Behavioral training
Continuous alternation task (Dataset1)
Mice were trained to continuously alternate in a custom-modified Figure 8 maze (theta maze: Figure 1A, left). Two days prior to maze training, mice were put on a water restriction schedule allowed to drink 1 mL/day. Before each session, mice were weighted and any sign of deteriorating health condition was monitored throughout the water restriction schedule. After full recovery from electrode implantation surgery, mice took from 5 to 10 days to reach the pre-surgery performance level of at least 40 alternations (min. 80 trials) after which recording sessions started. Reward (5–8 μL water) was delivered at the end of both side arms (Figure 1A) after each correct trial. Wooden doors were manually placed behind the animal at the end of the side arm to prevent the mouse to move backward and at the entrance to the opposite side arm.

Delayed alternation task 1 (Dataset2)
Details about training and task can be found in Huszar et al., 2022.[54] Briefly, water-restricted mice were trained to alternate in a modified Figure 8 maze for water reward delivered after every correct trial. Every trial was preceded by a 5-s delay. Three animals further

underwent exploration in novel environments (linear tracks, open fields and a T-maze) located in different rooms or parts of the room separated from the one used for the delayed alternation task. Optogenetic stimulation was always performed at the end of each recording session and never during behavior.

Delayed alternation task 2 (Dataset3)

Details about the task and training can be found in Zutshi et al., 2022.[27] Water-restricted mice were trained to alternate between left and right trials on a figure-8 maze. Each trial was separated by a 10-s long delay. Stimulation was targeted to the center arm in interleaved blocks of 10 trials. Stimulation started at the end of the delay and stopped once the mice crossed an infra-red beam detector located on the right and left arms.

Surgery

All mice in the *continuous alternation* group underwent a standard virus injection surgery targeting the medial septum and detailed elsewhere ([54]). Four to 8 weeks after virus injection mice were implanted with one or two silicone probes under Isoflurane anesthesia. After the loss of response to tail or foot pinch, skin above the calvaria was removed, the skull surface was cleaned from connective tissue and covered with UV-curable cement (Kerr's Optibond). After drying of the cement, one hole was drilled over the medial septal area, another above the right hippocampus and a third in the occipital bone for the ground/reference wire. A base composed of dental acrylic (Paladur, Kulzer International) was formed around the holes, a 105 μm core diameter optic fiber was lowered into the medial septum and attached by dental acrylic to the base. Medial septum was optically stimulated through this fiber in sessions *not used* in this study except in one animal in which virus injection was mistargeted thus optical stimulation did not affect hippocampal activity (via the septo-hippocampal pathway, see Table S1). Next, a silicone probe (see Table S1) already attached to a manually assembled microdrive (C-drive, see[55]) was positioned above the dorsal CA1 and the base of the drive was cemented to the skull by dental acrylic. In one animal two probes were implanted, each in one hippocampus. The microdrive-probe assembly as well as the optic fiber were surrounded by a copper mesh.

Details about surgery of mice used in the *delayed task* can be found in Huszar et al., 2022.[52] Briefly, Adult mice (3–6 months) underwent silicon probe implantation into their left or right dorsal CA1 (-2mm AP, +/− 1.7 mm ML), with details as described above. Each silicon probe- ASSY-156-E−1 (Cambridge NeuroTech), ASSY Int128-P64-1D (Diagnostic Biochips) or ASSY Int64-P32-1D (Diagnostic Biochips)- was attached to a 3D printed recoverable microdrive[56] and coupled with an optic fiber (105 μm core diameter, Thorlabs). The microdrive – probe – optic fiber assembly was surrounded by a 3D-printed head cap.

Details about electrode implantation for *Dataset3* is similar to that detailed above for *Dataset2* and can also be found in Zutshi et al.[27]

Recording of hippocampal activity

Five to seven days post-surgery, the probe was slowly descended into the pyramidal layer (usually in 3–4 days) identified by LFP ripples and sharp increase of spiking activity. Probes were left in place for several days until the deterioration of the multiunit signal, then moved about 75 μm (quarter turn of the drive screw) to record from a new set of neurons.

Spike sorting

For extracting waveforms corresponding to spikes of simultaneously recorded single units, we utilized Kilosort[57] followed by manual curation in Phy (https://github.com/cortex-lab/phy) and custom written plugins (https://github.com/petersenpeter/phy1-plugins). Kilosort clustering was performed with the following parameters: ops.Nfilt: 6*numberChannels, ops.nt0:64; ops.whitening:'full'; ops.nSkipCov:1; ops.whiteningRange: 64; ops.criterionNoiseChannels: 0.00001; ops.Nrank: 3; ops.nfullpasses: 6; ops.maxFR: 20000; ops.fshigh: 300; ops.ntbuff: 64; ops.scaleproc: 200; ops.Th: [4 10 10]; ops.lam: [5 20 20]; ops.nannealpasses: 4; ops.momentum: 1./[20 800]; ops.shuffle_clusters: 1. Unit isolation quality was judged during manual curation by inspecting i) the autocorrelogram for refractory violating events; ii) crosscorrelogram computed between the candidate and other clusters selected based on their similarity to the former; iii) shape of the cluster in the principal component space defined by the first two principal components. Occasionally, waveform clusters were split manually if judged to contain separable waveforms or clusters were merged if a clear refractory period (central trough) was possible to be identified on the crosscorrelograms of the events in them.

Neuron classification

In the continuous sessions, neurons were first classified based on firing rate criterion as putative pyramidal cells and interneurons. Next, the two groups were manually refined based on the presence of side peaks within 10 ms in their autocorrelogram indicating spike bursts, characteristic of pyramidal cells. In the delayed sessions (*Dataset 2*), a burstiness index was calculated as max(acg(0:10))/mean(acg(300:501)), where acg is the autocorrelogram with 1 ms binsize and ±500 ms lag.

Putative pyramidal cells with <100 spikes and putative interneurons with <1000 spikes per session were excluded from further analysis.

In the MEC-silencing dataset, units were separated into putative pyramidal cells and narrow waveform interneurons using their autocorrelograms, waveform characteristics and firing rate. This classification was performed using CellExplorer.[28]

Calculation of tuning curves

First, the maze was divided into 2-cm bins. Firing rate was calculated in these bins by N_i/T_i, where N_i = spike count in i^{th} bin, T_i = dwell time in i^{th} bin. The resulting tuning curves were smoothed first by oversampling along the spatial axis 100 times, using linear interpolation, then convolving the oversampled tuning curve with a 500-point Gaussian window (MATLAB's Gausswin function) corresponding to 5 bins (10 cm) and finally the smoothed tuning curve was downsampled back to the original spatial resolution.

Identification of place fields

Smoothed tuning curves were used for place field identification. First, a global threshold was defined as the mean of the smoothed tuning curve and every point exceeding this threshold was selected and the beginning and end of continuous supra-threshold segments were marked. Segments smaller than 3 bins (6 cm) were discarded. In the next step, it was determined whether the selected segments corresponding to putative place fields could be divided into more fields by locating local minima within them. If a minimum with <75% of the amplitude of the neighboring peaks was found, the segment was divided into two subsegments (two fields). Next, only fields with 50% higher amplitude than the global threshold (>1.5 x mean) were kept. Furthermore, place fields in which activity exceeded the 1.5 x global threshold but only in less than 10 neighboring trials were excluded. Finally, putative place fields with peak activity less than 5 times the out-of-field firing were also discarded.

Quantification of context-correlated activity

Selectivity index (SI). SI was defined as FR(i,x) – Trial(j,x)/Trial(i,x) + Trial(j,x), i: i^{th} even trial, j: j^{th} odd trial, i = j; x: x^{th} bin of the stem. A derived term, "Selectivity" is defined as abs(SI). While SI informs both about selectivity and its direction, Selectivity lacks directional information.

Dissimilarity index

Spatial bin-by-bin difference of left/right (correct, error) tuning curves expressed as the negative, 10-based logarithm of p-value calculated by Wilcoxon's ranksum test. Selectivity index combined with dissimilarity informs about both the extent, direction and statistical significance of context-selective activity in a given spatial bin. In all calculations, these measures were analyzed in place fields. Out of field segments were omitted.

Trial classification accuracy

After testing multiple classification models using MATLAB's *ClassificationLearner* application, an ensemble bagged tree classifier was selected for determining how accurately the trial-by-trial tuning curves (here, both in-field and out-field activity were included) predicted the behavioral choice of the mouse. Parameters of the classification: number of splits of the template tree was 197; number of learning cycles: 30; number of folds in cross-validated model: 5. Besides running on all trials, we also examined whether the model overfitted the data by classifying only the first half of sessions then using the output model parameters to test validity of classification on the second half of sessions. A graphical summary of these procedures is presented on Figure S1.

Clustering of place fields based on Selectivity and Dissimilarity

Instead of setting an arbitrary threshold of context-selectivity (thus forming a "low" and a "high" selectivity group), we examined whether clusters composed of differentially context-selective place fields could be formed based on Selectivity and Dissimilarity using K-means clustering. Place fields from delayed alternation sessions were clustered by using squared Euclidean distance whereas for clustering place fields from continuous alternation cosine similarity was used. Distance metric was selected by testing clustering using squared Euclidean, cityblock, cosine similarity and correlational distance and the metric resulting in the best clustering based on the maximal Silhouette value was selected. By using the selected distance metric 2 to 20 clusters were formed and Silhouette value for every clustering step was calculated. Cluster number indicated by the maximum Silhouette corresponded to the number of groups the place fields could be separated into with the highest intergroup distance. Parameters for K-means clustering (MATLAB's k-means function): number of replications: 100, number of iterations: 1000.

Retrospective – Prospective bias of neuronal activity

We have estimated if a neuron's activity was affected by the past or by the upcoming choice of the animal by correlation-based as well as a Dissimilarity-based procedure. For the correlation-based approach (Figures 4A–4E), tuning curve averages were generated by mean(TC_{Ttype}), where Ttype: correct left, correct right, error left, error right. Then, each single trial tuning curve in a session was correlated by Spearman rank correlation with these templates and an inferred context was assigned to the trial based on which template the given single trial tuning curve was correlated with the most (only correlation with p < 0.05 were used). This inferred context was then compared to the real context (or trial type) the animal was running in. This comparison resulted in one of four possible outcomes: match (inferred = real context), retrospective (inferred = previous trial's tuning curve, i.e., error right – correct left, error left – correct right), prospective (inferred = next trial's tuning curve, i.e., error left – correct left, error right – correct right), opposite (inferred = opposite real context, i.e., correct left – correct right, error left – error right). For sessions with a minimum of 5 error left and/or 5 error right trials, we have also implemented a Dissimilarity-based procedure: Dissimilarity index was calculated for every spatial bin between correct left/right and error left/right trials and minimum Dissimilarity was determined. We used here Dissimilarity for estimating the extent of similarity i.e., the more similar neuronal activity in two different types of trials was in a given spatial bin, the smaller the Dissimilarity between their tuning curves in a given spatial bin was. Based on the minimum Dissimilarity, we determined

the type of trial (context) a neuron's activity at a given location was the most similar to. Then, a Retrospective – Prospective bias was defined as (Dissimilarity$_{\text{error left – correct right; error right – correct left}}$ - Dissimilarity$_{\text{error left – correct left; error right – correct right}}$)/(Dissimilarity$_{\text{error left – correct right; error right – correct left}}$ + Dissimilarity$_{\text{error left – correct left; error right – correct right}}$). RP-bias = −1 corresponded to fully retrospective whereas +1 to fully prospective activity. Since this measure was calculated for every spatial bin, it enabled the analysis of within place field change of past/future choice-influenced activity.

Analysis of past/future-correlated population activity

As demonstrated on Figures S5G–S5K, population vectors (PVs) consisting of firing rate of simultaneously registered stem place cells were constructed for each spatial bin of the stem. Then, trial type templates were generated by averaging these PVs in each trial type resulting correct left, right, error left, right templates. These templates were correlated by Spearman rank correlation with PVs in every trial resulting in a position-resolved correlation map (Figure S5G small inset). Then, based on max(R$_{(\text{Position, Trial})}$) the trial type the template of which PV in a given position-trial was correlated with the most was determined generating an inferred context map (Figure S5H). Finally, this map was compared to the real context the animal was in, and an inferred vs. real context map was created (Figure S5I). Based on this map, the proportion of trials in which the population exhibited matching, retrospective, prospective or opposite activity could be calculated for each spatial bin (Figure S5J).

Identification of place cell assemblies

For identifying repeating patterns consisting of co-active neurons within a pre-defined time window, we have implemented the procedure detailed in Lopes Dos Santos et al. (2013).[33] We used theta cycles as time windows (instead of the generally used 25 ms time bins). First, we had generated theta cycle population vectors and then created a firing rate matrix from these theta cycle PVs. Firing rate values in this matrix were Z-scored. Next, a correlation matrix was generated by correlating the rows (corresponding to neurons) of this Z-scored firing rate matrix. Then, principal components of the resulting correlation matrix were calculated and the number of principal components contributing to up to 70% of explained variance were determined. For the PCA, MATLAB's built-in "pca" function was used. The next step was the rearrangements of principal component scores by independent component analysis (ICA). We utilized the "fastica" algorithm by Hugo Gavert et al. downloaded from https://research.ics.aalto.fi/ica/fastica/. This algorithm can calculate the PCA but it can also accept pre-calculated eigenvectors. Thus, we generated the eigenvalue decomposition of the correlation matrix by MATLAB's Singular Value Decomposition (svg) and fed the resulting eigenvectors and the number of principal components contributing to up to 70% of explained variance (determined by PCA, see above) to the fastica algorithm. As a result of ICA, we obtained vectors of scores (loadings) corresponding to the contribution of each neuron to the identified assembly. For each assembly, we sorted neurons based on the ascending order of scores and kept only those in the highest decile as significantly contributing neurons. Importantly, we excluded assemblies with less than 7 stem place cell members. We also calculated the reactivation strength of assemblies by generating the dot product of every pattern and the firing rate matrix consisting of the theta cycle population vectors. Finally, we converted theta cycle indices of assemblies (indicating in which theta cycle the given assembly was detected) to position, calculated assembly tuning curves for left and right trials by averaging position-resolved reactivation strength and determined Dissimilarity for quantifying the difference in reactivation strength between left and right trials.

Position estimation by template matching

For decoding the animal's position from simultaneously recorded place cells, a template matching approach was used.[32] First, population vectors composed of the firing rate of co-registered place cells was generated for every spatial bin in every trial. Three spatial population vector templates were built for each spatial bin by averaging population vectors from i) 10 randomly chosen trials (non-selective trials); ii) 5 randomly selected left trials; iii) 5 randomly selected right trials. Next, theta cycle population vectors were constructed from firing rates of co-registered place cells for every theta cycle. Every theta cycle population vector was correlated bin-by-bin with spatial population vector templates using cosine similarity (CS) and the one with the highest CS was chosen as the estimated position of the animal. Notably, cosine similarity resulted in better position estimation than Spearman's rank correlation if the number of simultaneously registered neurons was low (in continuous sessions) This procedure was repeated for non-selective, left and right templates. Finally, theta cycles co-occurring with the trials used for template building were removed. Decoding error for every theta cycle was determined by subtracting the real from the estimated position of the animal. Whether a given theta cycle is non-selective, left- or right-biased was decided based on the template that resulted in the smallest decoding error.

Identification of putative monosynaptic connections

Cross-correlograms (CCG) were generated from the within-place field spikes of pyramidal cells and simultaneously recorded interneurons using a maximum lag of ±100 ms and 1 ms time bins. To test whether cross-correlated neurons were connected monosynaptically, a hard threshold was set corresponding to the 1.5 times max(CCG$_{[1\text{ms}..90\text{ms}]}$). If a peak within 5 ms from the 0$^{\text{th}}$ time bin exceeded this threshold, the two neurons were assumed to be connected monosynaptically. A Monte Carlo simulation was also carried out by calculating crosscorrelograms between pairs of shuffled interneuron and place cell spike trains generated by randomly shifting spike times by a maximum of ±5 ms and real interneuron spike trains. Shuffling was repeated 1000 times. Significance level was set to 1% of the shuffled distribution for all bins. Two neurons were categorized as monosynaptically connected pair if a peak within the [0 ms–5 ms] interval of their CCG exceeded this threshold.[37] Finally, the CCGs of the selected significant pairs were

compared to those obtained by the hard threshold and based on this comparison the hard threshold method was proved to be stricter and used for identifying putative monosynaptically connected pairs.

Prediction of interneuron spiking by activity of place cells

We attempted to test whether spatial modulation of interneurons activity could be predicted by co-active place cell firing. Predictor variables were the trial-by-trial smoothed firing rate (from smoothed tuning curves) of all place cells, only putative monosynaptically connected and non-connected place cells whereas the response variable was the trial-by-trial smoothed firing rate of the interneuron. A robust linear regression model was fitted on the predictor and response variables after range normalization. The root-mean-square error was calculated as a goodness of fit measure for the model. Additionally, contribution of every potential predictor (place cell) was quantified by setting its value to a constant and comparing the resulting model to the full model (a "leave-one-out" strategy). Additionally, Selectivity of interneuron firing was also attempted to be estimated by the Selectivity of co-registered pyramidal cells by using the above-detailed methods. This analysis was performed by MATLAB's "fitlm" function.

QUANTIFICATION AND STATISTICAL ANALYSIS

In most of the cases median and interquartile range were given and box and whisker plots with outliers were plotted. Average ±standard deviation was provided where specified. For comparing unpaired data, Wilcoxon's rank-sum test was used. *: $0.01 < p < 0.05$; **: $0.001 < p \, 0.01$; ***$p < 0.001$. Comparison of multiple groups was done by Kruskall-Wallis ANOVA followed by Tukey-Kramer honest significant difference test. Details about more complex statistical models are given above in the respective STAR Methods section. Description of statistics can be found in figure legends except in few instances specified in the Results. All statistical tests were carried out using built-in MATLAB functions.